UC Davis
UC Davis Electronic Theses and Dissertations

Title

Complex DNA structures and their potential roles in molecular electronics

Permalink

https://escholarship.org/uc/item/1xn5k3mg

Author

Alangari, Mashari

Publication Date

2021

Peer reviewed|Thesis/dissertation

Complex DNA structures and their potential roles in molecular electronics

By

MASHARI ALANGARI
DISSERTATION

Submitted in partial satisfaction of the requirements for the degree of

DOCTOR OF PHILOSOPHY

in

Electrical Engineering

in the

OFFICE OF GRADUATE STUDIES

of the

UNIVERSITY OF CALIFORNIA

DAVIS

Approved:

_____

Joshua Hihath, Chair

_____

Erkin Şeker

_____

Weijian Yang

Committee in Charge

2021

i

Table of Contents

List of Figures

iv

v

List of Tables

Abstract

DNA structural stability and programmability offer innumerable degrees of freedom for the design and fabrication of DNA-based devices. DNA sequences can adopt complex structures beyond the double helix, and these structures can occur either naturally or artificially. A thorough understanding of the electrical properties of these intricate structures is still lacking and investigating the charge transport in these structures is of fundamental importance for developing DNA-based electronic devices or sensing platforms. This thesis examines the electronic properties of various complex DNA structures and the possibility of electrically identifying conformational differences using the single molecule break junction (SMBJ) method.

First, the conductance of an artificial DNA nanostructure, designed using DNA origami approaches, is examined. The single-molecule break junction (SMBJ) approach, which has been leveraged to examine charge transport through a variety of single-molecule devices, has been adopted to obtain the conductance of individual DNA origamis while bridging the gap between the SMBJ's electrodes. Thermodynamic analysis and molecular dynamic simulations suggest that the DNA origami used in this study is very stable. Also, different SMBJ tapping modes show that the DNA origami is highly conductive compared to double-stranded DNA.

Next, we systematically study the naturally occurring noncanonical guanine-quadruplex (G-quadruplex) structures and their transport properties by increasing the number of G-tetrads. We found that the conductance of the G-quadruplex is weakly length-dependent. These results suggest that the dominant transport mechanism is thermally activated hopping.

Finally, besides the G-quadruplex's essential regulatory role in biology, it is also the basis of many genetic diseases. Here, beyond the fundamental studies of DNA complex structures, we compare different tools for detecting G-quadruplex structures. In particular, circular dichroism

(CD), gel electrophoresis, and SMBJ were used to detect the presence of G-quadruplex structures. DNA sequences in this study show that the conductance value of the G-quadruplex is one order of magnitude higher than the double-stranded DNA. Therefore, harnessing electrical signals from individual molecules may provide the ultimate detection scheme for G-quadruplex.

Taken together, these experiments demonstrate that the structural polymorphism in DNA greatly influences the electronic properties, and one can foresee that complex structures will open doors to a wide variety of applications, including but not limited to molecular switches, sensors, and nanowires.

Acknowledgments

I consider myself as one of the luckiest graduate students to have Professor Joshua Hihath as my graduate advisor. I would like to thank him for his guidance, support, and encouragement over the past seven years. Professor Hihath's never ending enthusiasm for science has impressed and inspired me. I am truly grateful for his lenience and patience during research troubleshooting. I'm sincerely thankful to his constructive criticism during group or individual meetings. I would like to extend my appreciation and thanks to my committee members: Professor Erkin Seker and Professor Weijian Yang for the valuable feedback and suggestions.

My gratitude also extends to Professor Juan Manual Artes and Dr. Yuanhui Li for their help and support on conducting experiments during my first year; I would like to send my thanks to our collaborators: Professor M.P. Anantram, Professor Ersin Emre Oren and Busra Demir for their help on theoretical analysis; Professor Yonggang Ke for his help on the DNA origami design.

I would like to thank my friends and labmates: Dr. Haipeng (Billie) Li, Dr. Cliff McCold, Dr. Qiang Fu, Dr. Hyunhak Jeong, Dr. Bo liu, Professor Taher Ghomian, Professor Kübra Çelik, Lucas Domulevicz, Jonathan Marrs, Zahra Aminiranjbar, Yichen Gong, Macklin Bolton, Vincent Li, Roohi Ramachandran, Aaron Silman; as well as Professor Seker group: Dr. Jovana Veselinovic, Dr. Zidong Li, Dr. Tatiana Dorofeeva, Dr. Pallavi Daggumati, Noah Goshi, Gregory Girardi for the friendship and discussion.

Finally, I would like to thank my family; my parents for their support and love during my stay at the United States of America over the past nine years. I could have never achieved this without my family's encouragement.

To
My beloved parents,
My wife for never-ending love and support,
My son Faisal.

Chapter 1

Introduction and background

1.1. Introduction

The myriad of DNA's inherent properties renders it a potential candidate for molecular electronics. Concepts from chemistry, biology, and physics were combined in molecular electronics to understand the electronic properties and develop devices from molecules. The idea of integrating molecules as functional elements into solid-state devices originated from the seminal work of Aviram and Ratner[1], in which they suggest a molecular rectifier that consists of a donor and an acceptor separated by a bridge. The field of molecular electronics has grown in many directions, from the theoretical front to the experimental side. The invention of practical techniques, which allow the possibility of electrically contacting molecules, such as scanning tunneling microscopy (STM)[2–4], mechanically controlled break junction (MCBJ)[5,6], cross-wire techniques[7,8], and several other techniques[9–13] aid in the field's growth. Many groups worldwide have studied the charge transport properties through many molecules. They have established insights on the dependence of charge transport on the molecular length and chemical structure[14–22] and environment[23–25] using these experimental techniques. The molecular electronics society has focused on developing molecular-based devices analogous to conventional silicon-based electronics. Molecular field-effect transistor, in which a gate electrode can control current flow, requires the incorporation of a gate electrode into a two-terminal system, either using electrochemical gating in solution[26–28] or back gating in vacuum[29–31]. In addition, diode-like behavior, which allows current to flow in one bias direction, has been demonstrated in asymmetric molecular junctions[32–34].

Despite these developments in molecular electronics, interconnecting small molecules to develop molecular-based devices is still a significant challenge. This challenge stems from several factors. First, the search for long, highly conductive nanowires that interface with macroscopic electrodes and the molecular junctions is ongoing. Second, the physical limitation of the conventional lithographic technology is a significant hurdle for creating molecular-based electronic systems. However, the inherent properties of deoxyribonucleic acid (DNA) may offer the solution towards the ambitious goal of developing a DNA-based electronic device. One property is that DNA offers unique self-assembly properties with resolutions that overcome limitations in conventional lithographic technologies. A second property is the possibility of engineering complex DNA structures in which they may provide higher electrical conductivity than canonical structures.

This thesis will focus on three main objectives. The first objective is the study of the conductance of DNA origami. The second objective is to obtain the relationship between the conductance of the guanine-quadruplex structures and the length, and the final objective is the study of environmental impact on the G-quadruplex structure and its effect on the conductance.

This report will proceed with an introduction to the single-molecule break junction (SMBJ) technique, and essential concepts on charge transport models in molecular electronics will be introduced. A brief emphasis on the history of DNA conductance measurements is then presented. The second chapter will discuss the measurements of DNA origami electrical conductance. The third and fourth chapters will discuss the G-quadruplex molecules and the relationship between the conductance and the length, and the effect of surrounding ions on the G-quadruplex topology. Finally, the fifth chapter will provide a complete summary of the results discussed in the thesis and the future directions for this work.

1.2. Measuring single molecules

In 1959, Richard Feynman in his lecture "There's Plenty of Room at the Bottom" at the American Physical Society at Caltech introduced the idea of nanotechnology. This visionary speech inspired (and still inspires) many scientists such as Aviram and Ratner when they published their theory of a molecular rectifier[1] and Heinrich Roher and Gerd Binning for the invention of scanning tunneling microscope (STM)[2]. A slight modification had been made to the STM to read out electrical information for a single molecule at subnanometer length scales and give consistent results. Moreover, mechanically controlled break junction is another technique that is capable of measuring single-molecule electrical information, but, in the interest of brevity, one approach will be discussed in this report, and that is single-molecule break junction (SMBJ).

1.2.1. Single-molecule break junction (SMBJ) method

The conventional STM technique involves an atomically sharp tip that is brought close to a conducting substrate. When a bias is applied between the tip and the substrate, electrons tunnel through the solution or vacuum to the tip. Either monitoring the tunneling current or the distance between the tip and the substrate, the topography of the surface is imaged. From metallic point contact studies[35,36], Xu et al. at Arizona state university developed the SMBJ technique, which provides reproducible contacts between the molecules and the electrodes[4]. Also, this technique allows the collection of thousands of current traces in a relatively short period for performing statistics on the most likely molecular conductance. Many molecules have been investigated using the SMBJ techniques to obtain the conductance value.

In this thesis, all experiments were conducted at room temperature using a Molecular Imaging Pico-STM head connected to Nanoscope IIIa controller from Digital Instruments. The

preamplifiers used in all experiments were lab-built with various gains. The movement of the STM tip is controlled by a lab-built program using LabVIEW from National Instruments with a PCIe-6363 data acquisition (DAQ) card.

In an SMBJ experiment, one uses a gold tip, gold substrate, and a Teflon cell to hold fluid on the gold substrate. When a quantity of modified molecules with linkers that bind to the gold electrodes is inserted into the solution, the molecules can form a molecular junction. The formation of a molecular junction is achieved by bringing the gold tip to the gold substrate until the current saturates the preamplifier, then the tip is retracted until the current reaches the lower limit of the preamplifier. Recording and monitoring the current-distance traces during the retraction process, in the absence of molecules, one observes a smooth exponential decay as expected for a charge tunneling through the intermediate. On the other hand, when modified molecules with linkers are present in the intermediate, molecules will bridge the gap between the gold electrodes, and a step-like feature or a 'plateau' appears in the current-distance traces see figure 1.1.
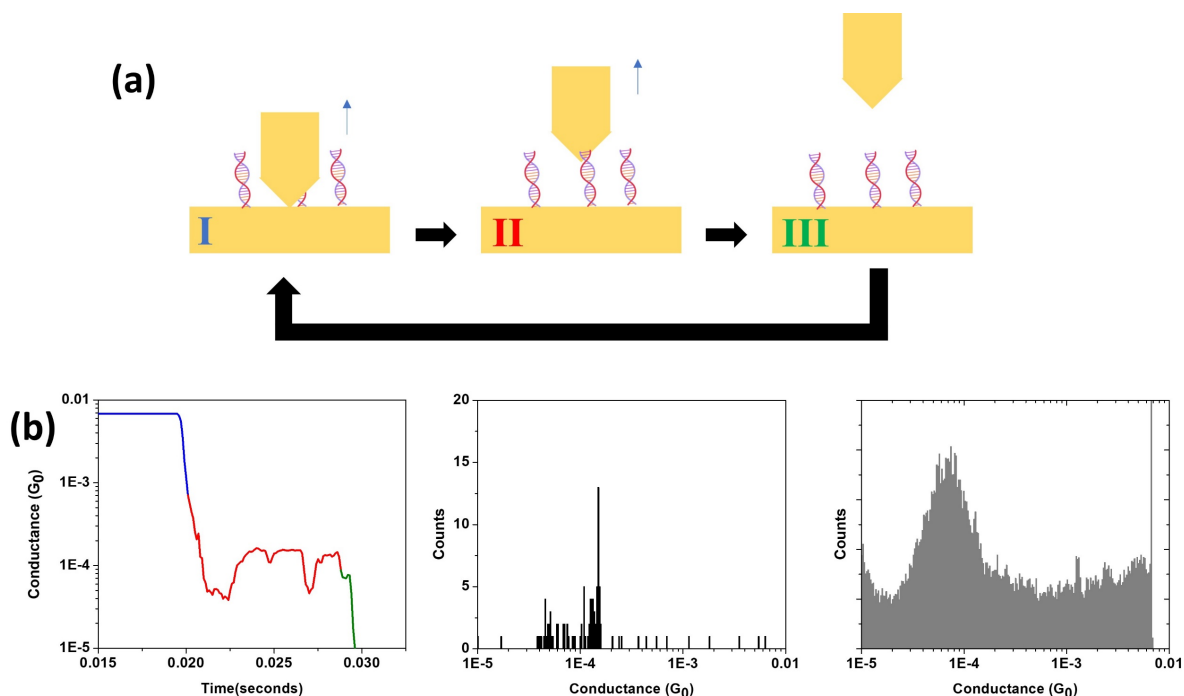
Figure 1.1: Schematic representation of the SMBJ method (a) the gold tip is brought into contact with gold substrate until the current saturates. Then the tip is retracted at a fixed rate until the current reaches the minimum setpoint. Then, the whole tapping process is repeated thousands of times. (b) left panel: single trace with a step-like feature that is color-coded at each stage at (a); middle panel: single histogram of the single trace; right panel: conductance histogram of the dsDNA with a peak that is composed of hundreds of single traces with step features.

An automated lab built LabVIEW program from National Instruments for data analysis. The LabVIEW program selects current-distance traces with steps that satisfy three criteria. First, a linear fitting to each current-distance trace on a semi-logarithmic plot then selects traces with fitting residuals above the specified value (typically 0.25). This criterion removes smooth exponential traces. Second, a logarithmically binned histogram was created for each single current-distance trace. If the number of counts is above a specified threshold value (typically 6-13 counts), then it is selected. Finally, the single trace is selected if the summation of the total number of counts in a single trace histogram is below a specified value (typically 500-800). If the three criteria apply to a single trace, it would be added to the overall conductance histogram, which identifies that molecular junction's most probable conductance value.

1.2.2. SMBJ experimental preparation

1.2.2.1. Gold substrate preparation

The evaporator used in our lab was modified with a halogen light bulb to control the temperature of the mica while the gold is being evaporated. Gold substrates were prepared by thermally evaporating 130 nm of gold (ACI Alloys, 99.999% purity) on a freshly cleaved mica surface under a vacuum of ~10^{-7} Torr and a temperature of 350ºC. After the deposition, the gold substrates were

transferred into individual vials and stored under vacuum before the experiment. Prior to each SMBJ measurement, the gold substrates were flame-annealed using butane flame for less than 1 minute to clean and anneal the surface.

1.2.2.2. SMBJ tip preparation

The SMBJ tip was prepared by mechanically cutting a gold wire (Alfa Aesar, 99.999% purity, 0.25mm diameter) to form a needle-like end. For insulating the tip, a copper plate (1-cm^2) with a ~0.1 cm^2 rectangular gap extends from one side to the center of the plate is attached to a soldering iron. Apiezon wax (Ted Pella Inc.) is melted on the plate. The tip is brought to the wax from underneath the gap using a manipulator. The tip is immersed in the wax for ~ 30seconds to allow the wax to adopt the tip's shape. Then, the tip is slowly raised through the wax. A well-insulated tip in a buffer solution results in a leakage current of less than 10pA.

1.3. Charge transport models in molecular electronics

Theoretical models for charge transport in a single molecule are essential for predictions and explain the experimentally measured electrical properties. The following section will detail some basic models for charge transport in molecular systems. The section starts with the Landauer formula, which treats charge transport in mesoscopic scale systems as a scattering process, then followed by brief discussions on the superexchange and incoherent tunneling models in a molecule bridged between two electrodes under applied voltage, and finally will introduce a coherence-corrected hopping model.

1.3.1. The Landauer formula

In a macroscopic system, Ohm's law describes the electrical conductance of a metallic wire, which states that the current is proportional to the applied bias. The conductance is the proportional constant and it is given by:

$$G = \sigma \frac{A}{L}$$

Where σ refers to the conductivity, which is a specific property to a material. A is the cross-sectional area of the conductor. L is the length of the conductor. When the size of the conductor reaches smaller length scale, that is mesoscopic system, the conductance ratio will reach infinity due to the inverse length relation. Therefore, quantum coherence plays a significant role in the transport properties of atomic-sized conductors. There are different transport regimes in mesoscopic systems depending on multiple length scales; these length scales are determined by different scattering processes. For instance, phase-coherence length, L_φ, describes the distance in which the information about the electron's phase is preserved. The inelastic scattering, such as the interaction between the electron-electron or electron-phonon, leads to the destruction of the phase coherence. When the length of the sample is smaller than L_φ, the sample is said to be in the mesoscopic regime. Another important length scale is the electron mean free path γ, which refers to the distance that the electron can travel in a sample with constant momentum. When the sample length is larger than the γ, the sample is in the diffusive regime where the motion of the electron is like a random walk with a step size of γ between elastic collisions with impurities. On the other hand, when the sample size is smaller than γ, the sample is in the ballistic regime where the electron momentum is preserved, and the electron scatters with the boundaries of the sample.

In a typical transport experiment, a molecule is bridged between two electrodes under a fixed voltage. In this system, the electrodes act as electron reservoirs where electrons are free to

propagate in plane waves. There are two probabilities for incident electrons on the molecular junction, either electrons tunnel through the molecular junction, a barrier, or scattered backward. The idea of describing the transport in such systems as a transmission process with scattering and reflecting was first introduced by Rolf Landauer[37]. He showed that in electrode-molecule-electrode junctions, the conductance is a transmission. Mathematically, the formula is

$$G = \frac{2e^2}{h} \sum_{n=1}^{N} T_n(E) = G_0 \sum_{n=1}^{N} T_n(E)$$

The first term, $G_0 = 77.5\mu S$, is the conductance quantum and can be seen in a gold quantum point contact study. The second term is the summation of all probabilities through the junction for all modes.

1.3.2. Superexchange tunneling

The transition operator that describes a system of n discrete energy states confined between two available states (see figure 1.2) is defined in the limit of tight binding and weak coupling as:

$$T_{LR}(E) = V_{LR} + V_{L1}G_{1n}(E)V_{nR}$$

V_{LR} defines the coupling between the left and right electrodes. The second part of the equation describes the charge transport from the left electrode through the bridge to the right electrode. V_{L1} and V_{nR} represent the coupling between the left electrode to the first energy bridge state and the last energy bridge state to the right electrode, respectively. G_{1n} is the Green's function from the first bridge site to the last one, which is:

$$G_{1n}(E) = \frac{1}{E - E_n} \prod_{i=1}^{n-1} \frac{V_{i,i+1}}{E - E_i}$$
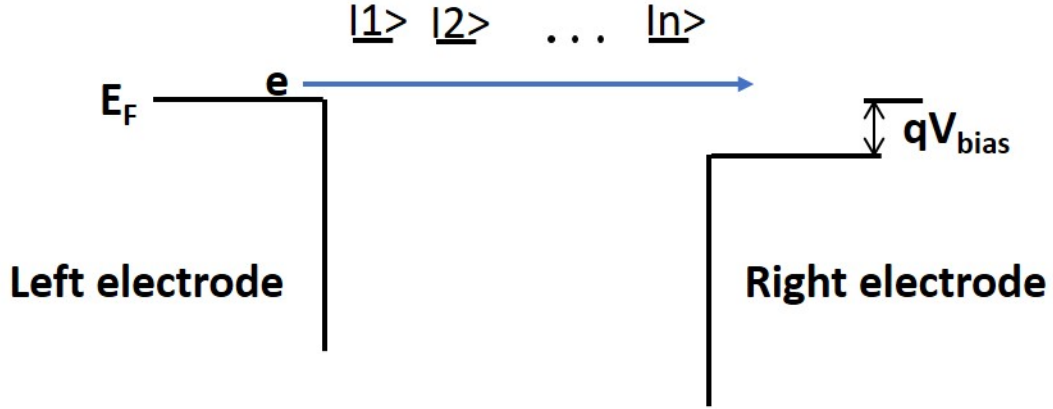
Figure 1.2: Energy band representation of a molecule bridged between Left and right electrodes, and V is a bias between the left and right electrodes. The arrow represents a charge tunneling through the molecule from the left to right electrodes. For simplicity, energy levels are degenerate.

To simplify the above equation, assume the energy levels are degenerate, i.e., $E_i = E_B$, and the coupling energy between the energy states is the same ($V_{i,i+1} = V_B$). The simplified equation is as follow:

$$G_{1n}(E) = \frac{1}{V_B}\left(\frac{V_B}{E - E_B}\right)^n$$

The term V_{LR} can be ignored because the coupling between the left and right electrodes is relatively weak. The transition operator is then described as:

$$T_{LR}(E) = V_{L1}\frac{1}{V_B}\left(\frac{V_B}{E - E_B}\right)^n V_{nR}$$

The conductance after applying the Landauer formula is as follow:

$$G = G_0\bar{T}(E_F)$$

The constant $G_0 = \frac{2q^2}{h}$ represents the conductance quantum and $\bar{T}(E_F)$ describes the transition coefficient which is:

$$\bar{T}(E_F) \propto e^{-\beta l}$$

Where $\beta = \frac{2}{a}\ln(\frac{E-E_B}{V_B})$ is the exponential decay constant that describes the potential barrier. The length of the molecule or the bridge is l that is the distance between the left and right energy state, which is na where a is the distance between two adjacent energy states. The final conductance of the system is:

$$G = G_0 e^{-\beta l}$$

1.3.3. Incoherent hopping

The other mechanism that explains charge transfer through the molecular junction is the incoherent hopping model, which is dominant in long-range transfer. Incoherent tunneling loses the phase information of the transported charge through the molecule as opposed to coherent tunneling, where phase information is preserved. In other words, the traversal time of the charge is considerably larger than the time scales associated with the scattering interactions. Hopping is defined as a combination of multiple "hops" in which the charges are localized at specific sites along the length of the molecule (see figure 1.3). As opposed to superexchange tunneling, hopping has a much weak length dependence.
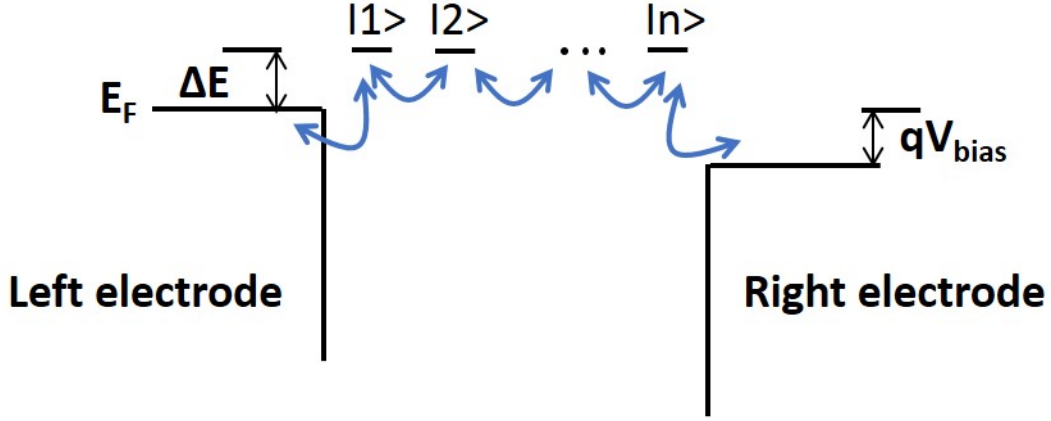
Figure 1.3: Energy band representation of a molecule bridged between Left and right electrodes. V is the bias between the left and right electrodes. ΔE represents the difference between the first energy state and the left electrode. The arrows represent charge transfer between sites.

In figure 1.3, the molecule has n energy states, and ΔE is the difference between the first energy state on the molecule and the electrodes known as the activation energy. The incoherent hopping rates between the energy states on the bridge are determined by k_{ij} (from state j to state i). The steady-state current between the state j and state $j+1$ is as follow:

$$I_j = q\left(k_{j+1}P_j - k_{j,j+1}P_{j+1}\right)$$

Where P_j and P_{j+1} are the probabilities of occupations the corresponding energy states. The rate of the occupation probability is expressed as:

$$\dot{P}_j = \frac{dP_j}{dt} = -\left(k_{J-1,J} - k_{J+1,J}\right)P_J + k_{J,J-1}P_{J-1} + k_{J,J+1}P_{J+1}$$

For $j = 0$ and n, the probabilities are the Fermi level of the left (f_L) and right (f_R) electrodes, respectively. Assuming the system is in steady-state, which means $\dot{P}_J = 0$. Also, all the transfer rates on the bridge are the same $k_{j,j+1} = k$ and the following:

$$k_{1,0} = k_L e^{-\Delta E/k_b T}; \ k_{0,1} = k_L$$

11

$$k_{n,n+1} = k_R e^{-(\Delta E - qV)/k_b T}; \ k_{n+1,n} = k_R$$

After substituting the assumptions above in the current equation and the final conductance equation

for hopping that shows weak length dependence is described as follow:

$$G = \frac{q^2}{k_b T} \left[\frac{e^{-\Delta E/k_b T}}{\frac{1}{k_L} + \frac{1}{k_R} + \frac{(n-1)}{k}} \right]$$

1.3.4. Coherence-corrected hopping

Incoherent transport relies on energy imparted by phonons to facilitate for charge carriers to hop

from one site to another of slightly higher energy. The charge carrier loses information about their

phase with each hop; hence, the transport is incoherent. Previously, it has been suggested that

coherence length, which is the distance for a charge carrier to travel without loss of phase

information, for DNA is longer than a single base pair. Recently, Li et al. showed that the

coherence length for DNA: RNA has been estimated at 5bp[38]. Another work by Xiang et al.

estimates the coherence length for dsDNA is 2bp[39]. These results suggest an intermediate charge

transport mechanism between tunneling and hopping.

In 1988, Marcus Büttiker developed a model that includes a coherence correction to an entirely

incoherent charge transport system[40]. Figure 1.4 represents a schematic for the intermediate

transport mechanism. Multiple adjacent energy states are grouped together to form one superstate.

In the superstate, the charge can transport coherently, and phase information is preserved.

However, the charge will hop between the super states. The total resistance of the coherent-

corrected hopping transport is given by:

$$R_{tot} = R_0 + \frac{h}{e^2} \frac{(N-1)}{1 - 2e^{-B(N-1)} \cos[C(N-1) + \Delta\varphi]} T_{PP}^{-1}$$

Here R_0 is the contact resistance, h is the plank constant, e is the electron charge, N represents the number of hopping sites, T_{pp} is the average transmission from one purine site to an adjacent one. $B = \lambda_0/v\tau_i$ reflects the decay of coherence over distance, λ_0 is the rise per base pairs in double-helical DNA, $v\tau_i$ is the coherence length, where v is the velocity of the carrier and τ_i is the inelastic scattering time, $C = 2\sqrt{2mE}/\hbar\lambda_0$ where m and E are the mass and energy of the charge carriers, respectively, and $\Delta\varphi$ is the phase shift of the carriers.
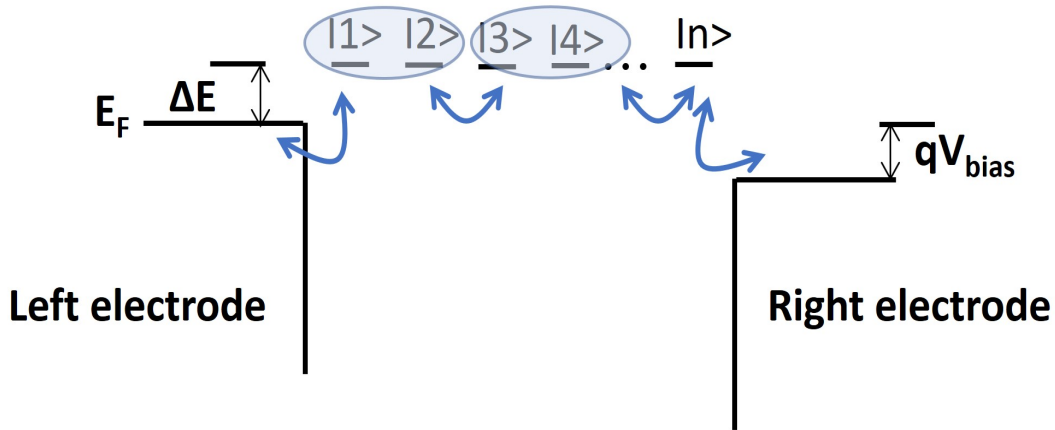
Figure 1.4: a visual representation of the coherent-corrected hopping. The shaded blue ovals are schematics of two superstates.

1.4. Circular dichroism (CD) of DNA

In the 19th century, a French scientist named Aimé Cotton was the discoverer of circular dichroism (CD) as a graduate student by experiment[41,42]. He measured, what was called the Cotton effect and CD later, a solution of potassium chromium tartrate and potassium copper tartrate. The resulted spectra are equal in amplitude but opposite to each other, which he avoided the uncertainty of the previously measured amethyst by Haidinger and Dove[41]. CD spectroscopy is a very useful tool to

13

investigate the structures of DNA. The asymmetric DNA backbone sugars and the helical arrangement of DNA bases interact differently with circularly polarized light.

1.4.1. Circular Dichroism method

Circular dichroism is an absorption spectroscopy technique that detects the differential absorption between the left and right circularly polarized light. CD uses ultraviolet (UV) light to investigate chiral molecules, which preferentially absorb one circularly polarized light over the other. The CD spectrum is usually reported in millidegrees which is directly related to the difference in absorption of left and right circularly polarized light. In a CD machine, there are four essential components. A high-intensity light source that gives white unpolarized light and a monochromator that outputs linear polarized light with a specific wavelength. Moreover, the photoelastic modulator (PEM) receives a linear polarized light and breaks it into right and left circularly polarized light RCP and LCP, respectively. The circularly polarized lights pass through the sample chamber and at the end of the chamber there are two photo multiplier tubes (PMT) that quantify the light absorption due to the sample (see figure 1.5). When the electric field components of the two propagating circularly polarized lights with equal amplitudes combine, the superposition of the electric field is linearly polarized. However, in a chiral medium, RCP and LCP will be absorbed by the medium in a different amount; therefore, the superimposed light is not a linear but elliptically polarized light (see figure1.6).
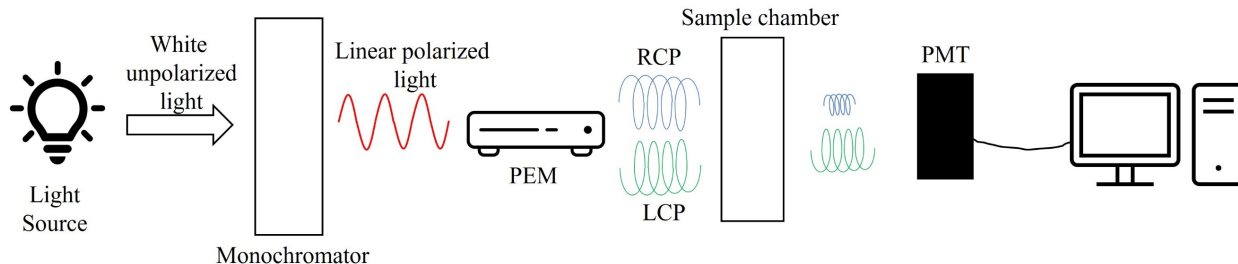
Figure1.5: The main components of the CD instruments with the evolution of light from unpolarized to the two components of circularly polarized. RCP and LCP are spatially separated.

There are multiple ways to report the CD spectrum. The CD spectrum in this thesis is reported in millidegrees which is referred to the ellipticity of the superimposed light that is given by[43–45]:

$$\tan\theta = \frac{|RCP| - |LCP|}{|RCP| + |LCP|}$$

Where $|LCP|$ and $|RCP|$ are the amplitudes of the right and left circularly polarized vectors.

In practice, instead of ellipticity, we can measure the intensities of the lights at the detectors, and Beer's law describes the intensity of light:

$$I = I_0 \, e^{-A\ln(10)}$$

Where I_0 is the incident light on the sample, and A is the amplitude of the absorption light.

Also, the ellipticity is very small and assume that $\tan\theta \approx \theta$ this gives:

$$\theta = \frac{\sqrt{I_{RCP}} - \sqrt{I_{LCP}}}{\sqrt{I_{RCP}} + \sqrt{I_{LCP}}}$$

Gives:

$$\theta = \frac{\sqrt{I_0}e^{-\frac{A_{RCP}}{2}\ln(10)} - \sqrt{I_0}e^{-\frac{A_{LCP}}{2}\ln(10)}}{\sqrt{I_0}e^{-\frac{A_{RCP}}{2}\ln(10)} + \sqrt{I_0}e^{-\frac{A_{LCP}}{2}\ln(10)}}$$

Simplifies

$$\theta = \frac{e^{\frac{A_{LCP}-A_{RCP}}{2}\ln(10)} - 1}{e^{\frac{A_{LCP}-A_{RCP}}{2}\ln(10)} + 1}$$

Using Taylor series

$$\frac{e^x - 1}{e^x + 1} \approx \frac{x}{2}$$

The final measure in radians is

$$\theta = (A_{LCP} - A_{RCP})\frac{\ln(10)}{4}$$
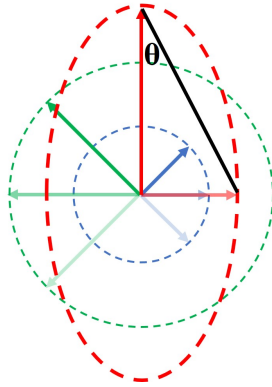
Figure 1.6: a diagram of the elliptically polarized light (red, electric field) as a result of the superposition of left (green) and right (blue) circularly polarized light. **θ** is the angle between the maximum and minimum electric field vectors.

1.4.2. Double-stranded DNA structures and CDs

DNA is a polymer made from chains of nucleotides. Each nucleotide is composed of a five-carbon sugar molecule attached to a phosphate group and a nitrogen-containing base. The bases in DNA are guanine (G), adenine (A), cytosine (C), and thymine (T) (figure 1.7).
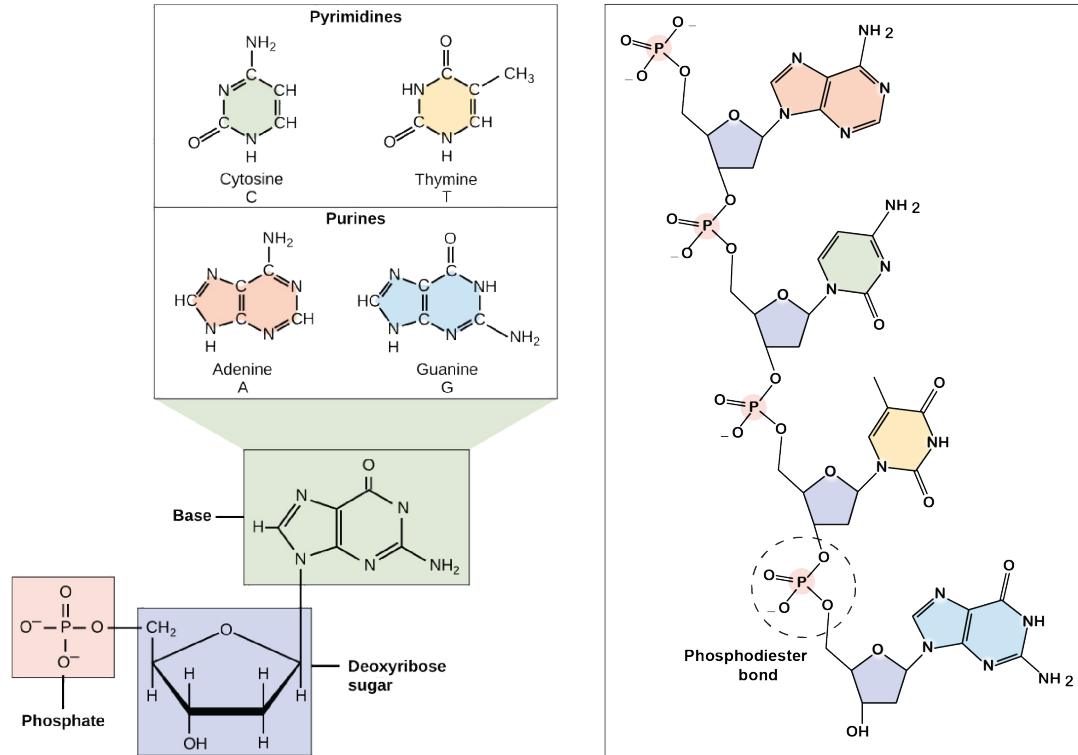
Figure1.7: Illustration of the DNA nucleotide, the four DNA bases, and the backbone of the DNA. Photo credit: Khan Academy[46].

The DNA backbone is built by alternating the sugar and phosphate groups, which defines the directionality of the DNA. Each nucleotide is linked to another by a chemical bond, called a phosphodiester bond, between the sugar and the adjacent phosphate group (see figure 1.7: right panel). The asymmetry of the backbone leads to directional DNA, whose sugar and phosphate groups are labeled as 3' and 5' ends, respectively. The 3' and 5' refer to the number of the carbon atoms in the sugar molecules to which the hydroxyl-group and phosphate-group bond, respectively. Single-stranded DNA can bind to another antiparallel single-stranded DNA by hydrogen bonds between each base pair, i.e. A to T and G to C, to form double-stranded DNA. There are three hydrogen bonds between G and C, while there are two between A and T. Thus, melting temperature for double-stranded DNA rich in GC content is higher than in one rich in AT.

17

Double-stranded DNA (dsDNA) adopts multiple conformations, namely A-, B- and Z-forms. They are grouped based on their helical twist. The right-handed helical group contains the most common form that exists in nature B-form and A-form see figure 1.8, and the left-handed group includes the Z-form. There are differences between each form, and they are summarized in TABLE 1.
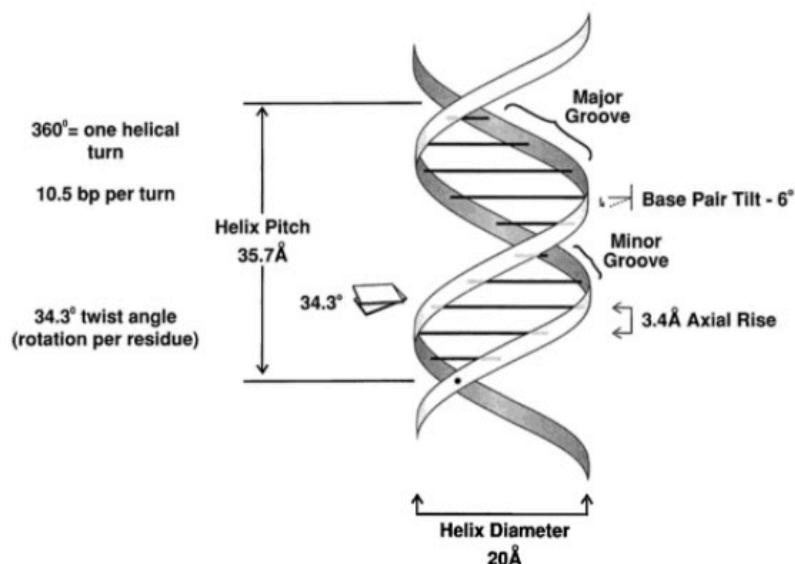
Figure 1.8: Illustration of the right-handed helix twist B-form DNA and some of the structural parameters[47]

Table 1.1: DNA helix parameters[47]

Parameter	A-form	B-form	Z-form
Helical twist	Right-handed	Right-handed	Left-handed
Base pair (bp) / turn	11	10.5	12
Axial raise (Å)	2.55	3.4	3.7
Base pair tilt (º)	20	-6	7

Diameter of the helix(Å)	23	20	18

The A-form is most commonly found in RNA; however, DNA may adopt the A-form in the presence of ethanol. Also, DNA rich in GC bases exhibits the A-conformation[48,49]. In CD spectra, a positive band at 260 nm and a negative band at 210 nm characterizes the spectrum of A-form (see figure 1.9A Right panel). Synthetic and natural polydeoxynucleotides adopt the so-called B-form with common global features. A positive band at 280 nm and a negative band around 245 nm characterizes the B-conformation. Depending on the sequence, the CD spectrum may differ because of differences in chromophores and conformational properties[50]. For instance, DNA with only AT bases adopt an unusual B-form due to the high propeller twist AT base pairs[51,52]. DNA may transition from B-DNA to A-DNA and vice versa in the presence of ethanol(figure 1A left panel)[48,50,53]. In 1972, Pohl and Jovin discovered the left-handed DNA helix while studying the effect of the ionic strength on the poly[d(GC)][54]. It was named Z-DNA because of the zig-zag path of the sugar-phosphate backbone[55,56]. The CD spectrum of the Z-DNA is approximately an inversion of the B-DNA spectrum; it exhibits a negative band at 290 nm, a deep negative band at ~205 nm, and a positive band at 260 nm; there are several variants of the Z-DNA and all of them possess the deep negative 205 nm (see figure 1B right panel). The transition between Z-DNA and B-DNA or A-DNA is possible in the presence of alcohol (see figure 1B left panel).
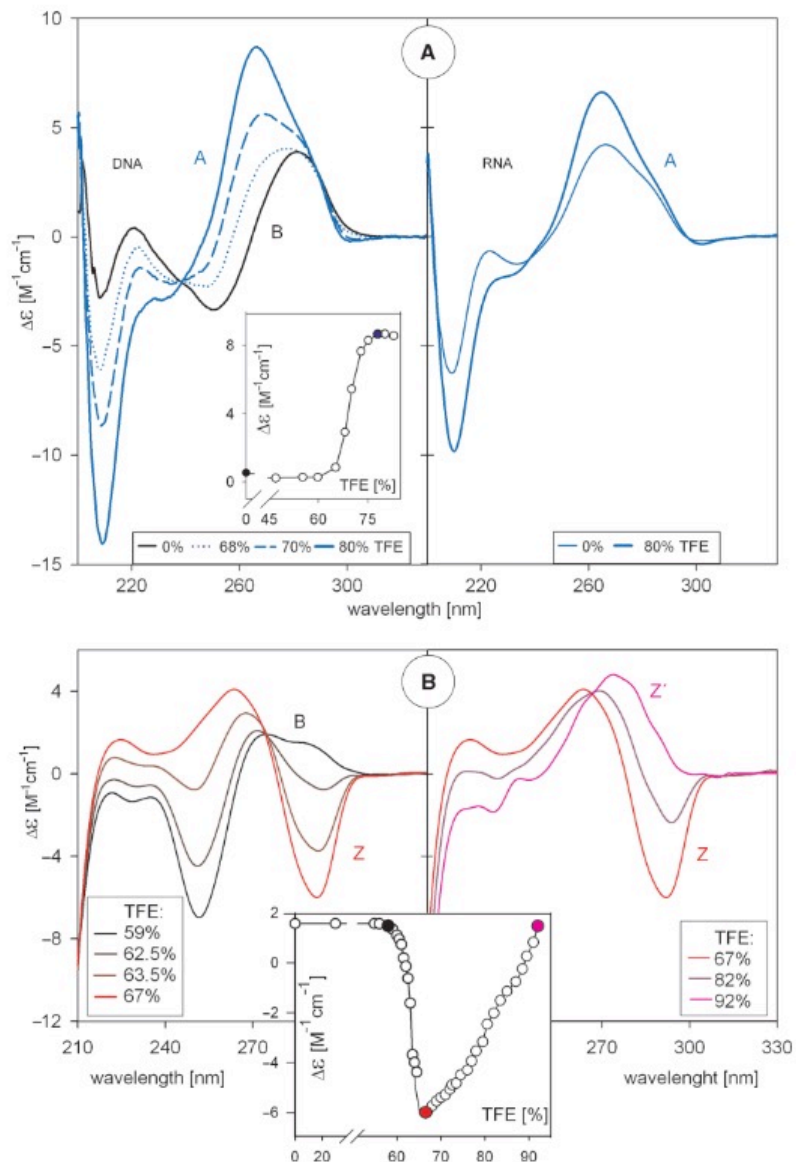
Figure 1.9: CD spectra for A-form, B-form, and Z-form of DNA and transitions between forms. The Y-axis is the difference in extinction coefficients, that are related to absorbance using Beer's law, between left and right circularly polarized light (A) left panel: transition between B-DNA to A-DNA in the presence of trifluoroethanol (TFE). Right panel: RNA spectra with and without the TFE. Insert: transition monitored at 266 nm as a function of TFE concentration. (B) left panel: transition between B-DNA to Z-DNA in the presence of trifluoroethanol (TFE). Right panel: Z-DNA to Z'-DNA transition in the presence of TFE. Insert: transition monitored at 291 nm[50].

1.4.3. G-quadruplex structures and their CDs

Nucleic acid sequences with three or more consecutive guanine bases tend to form G-quadruplex structures[57]. These structures comprise guanine tetrads (also known as G-quartets) bounded by Hoogsteen hydrogen bonds (Figure 1.10). The tetrads are stacked, and the stability of the G-quadruplex depends on the cation type inserted between the tetrads. In general, the G-quadruplex is stable in the presence of metal cations such as potassium and sodium[58]. G-quadruplexes can be in a parallel or anti-parallel orientation and monomolecular, bimolecular, and tetramolecular. CD spectroscopy of G-quadruplex structure detect only global features of the molecule, and for in-depth analysis of the structure, a combination of other techniques such as NMR or X-ray crystallography is preferred. The appearance of specific bands in a CD spectrum reflects the populations of the guanine bases' anti and syn glycosidic bond in a particular G-quadruplex arrangement (Figure 1.10b).
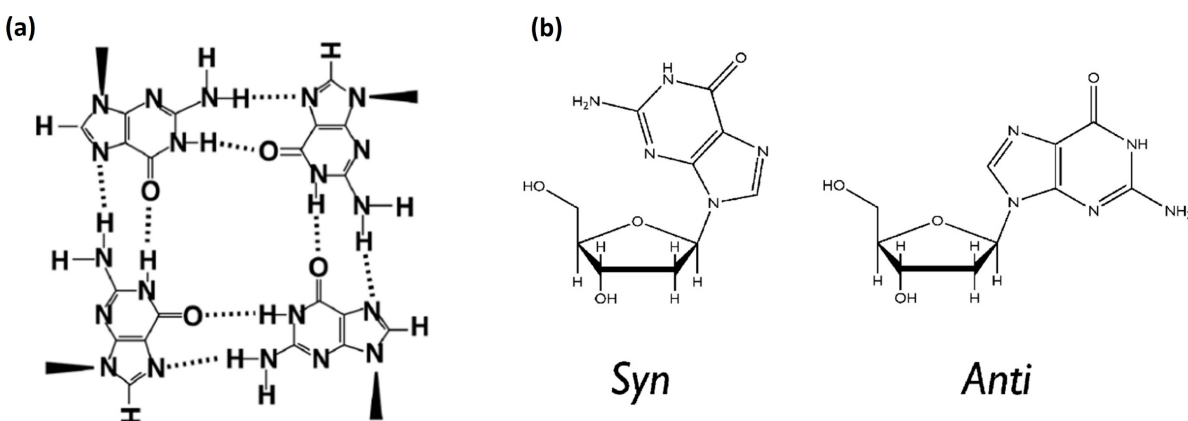
Figure 1.10: Schematic representation of (a) G-quartet[59] and (b) syn/anti guanine conformations[60].

Although the dominant technique to study the G-quadruplex structures is NMR spectroscopy, CD spectroscopy is mainly used to study the G-quadruplex structures empirically. The complexity of

the theoretical description of CD spectra for G-quadruplex to gain information about the molecule structure at the atomic level is a major hurdle from advancing in the study of G-quadruplex structures. Therefore, a complete understanding of a G-quadruplex structure requires CD spectrum, NMR, and X-ray results. G-quadruplex structures can be categorized into two types. The main features of a parallel G-quadruplex structure, despite the number of strands comprising the structure, have positive bands at 260 nm and 210 nm and a negative band at 240 nm[50,61,62]. The DNA sequences of 8 consecutive guanines, G_4TG_4 and $G_4T_2G_4$, adopt the parallel G-quadruplex structure see figure 1.11a. The anti-parallel type has two positive bands at 290 nm and 210 nm and a negative band at 260 nm. The distinct features in CD spectra between the two types originate from the different stacking of the guanines with different glycosidic angle conformations[63,64]. The features of antiparallel G-quadruplex structures are similar whether G-quadruplex was formed by bimolecular or monomolecular[59,65,66]. Two hairpin dimers form bimolecular G-quadruplex with different loop locations. For example, $G_4T_4G_4$ and $G_4T_3G_4$ adopt anti-parallel two-hairpin structures with diagonal and lateral loops, respectively, and the CD spectra in figures 1.11a and b for both G-quadruplexes share indistinguishable features[67,68].
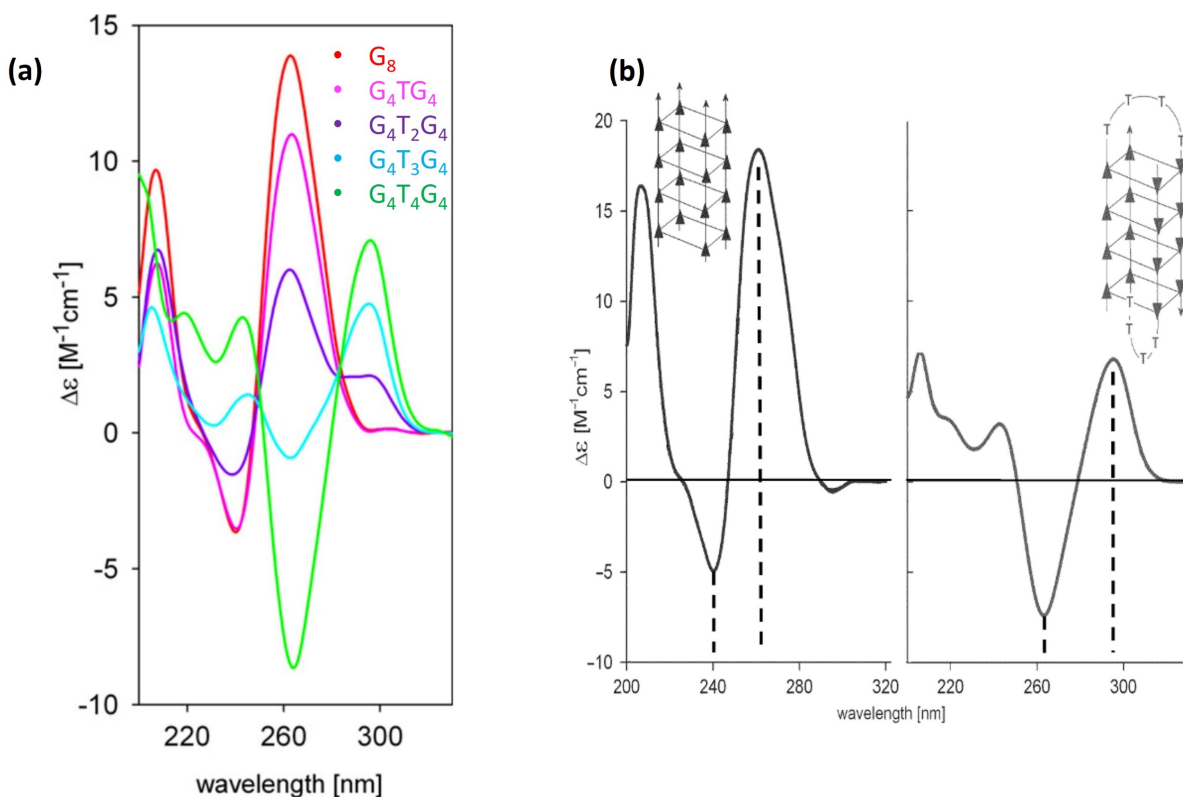
Figure 1.11: CD spectra of multiple G-rich sequences adopt G-quadruplex structures (a) the effect of increasing the loop length on the G-quadruplex structures and (b) parallel and two-hairpin dimer with diagonal loop.

1.5. History of DNA conductance studies

The DNA bases are similar to benzene molecules in structure. Therefore, delocalized π bonds or antibonding π^* states are formed by the atomic orbitals P_z of the carbon atoms (z is the direction perpendicular to the plane of the molecule). When the spacing between two adjacent π-orbitals is close, a coupling occurs, and a conduit for charge transport along the DNA helical axis is created. In the past two decades, direct conductance measurements of dsDNA or DNA: RNA hybrids using SMBJ have been reported. Also, conductance measurements of G-quadruplexes using conductive atomic force microscope (CAFM) or mechanically controlled break junction (MCBJ) techniques

23

have been published. The conductance value of a relatively short dsDNA depends on many factors, such as the environment where the measurement is conducted and the molecule's conformation. This section highlights some of the experimental works on DNA conductance studies.

Conductance measurements of DNA in an aqueous environment vs. dry conditions suggested that better base pair stacking and stable DNA conformation are essential for DNA conductivity, and it is achieved while DNA is in buffer conditions. Tran et al. published a study comparing the λ-DNA (a linear dsDNA extracted from Escherichia coli or E.coli) conductivity in buffer solution vs. dry condition and concluded that the conductivity is about one order of magnitude higher in buffer conditions compared to a dry environment.

Charge transport through dsDNA depends on the DNA sequence. In 2015, Limin et al. reported that the single-molecule conductance of self-complementary DNA duplexes with alternating G and stacked G bases adopt different transport mechanisms. The conductance of the alternating G bases was found in good agreement with previously reported results that the charge transport is hopping which indicates a weak length dependence. In contrast, the stacked G bases sequences showed an oscillation in their conductance as the length of the sequences increased. Theoretical simulations derived from Buttiker's theory suggest that the oscillation on the conductance value is due to partially coherent and partially hopping charge or coherent-corrected hopping transport. The simulations found that the highest occupied molecular orbitals (HOMO) in the stacked G are delocalized over multiple G bases. Another study by Xu et al. showed that by inserting AT bases into GC-rich sequences, conductance decreases exponentially with adding more AT bases, indicating coherent tunneling. On the other hand, the conductance of the alternating GC sequences showed a weakly length-dependent suggesting a hopping mechanism for charge transport.

As discussed earlier that stable DNA conformation is critical for conductivity; dsDNA adopts a variety of conformations. Wang et al. studied an alternating $(GC)_4$ dsDNA using the SMBJ technique and induced structural transition from B-to Z- conformations by increasing the concentration of Mg^{2+} ions. The conductance value decreased by two orders of magnitude as the conformation changed from B- to Z-form. The transition causes an increase in the distance between base pairs and a flipping of the G bases by roughly 180º; therefore, disruption of the π-π orbital stacking between adjacent base pairs occurs. Moreover, Artes et al. explored the effect of B- to A-transition on the conductance value. The sequence in this study is $CCCG(CG)_2CCC$, and the transition from B- to A-form was induced by adding 80% ethanol. The conductance value increased by one order of magnitude when the molecule adopted the A-conformation. Ab initio and electronic density of states calculations of the two conformations suggest that HOMO is distributed over 70% of molecular length in A-form and 50% in the B-form, leading to higher conductance of A-form DNA.

Conductance measurements of a single G-quadruplex molecule have also been conducted using break junction techniques. In the research study conducted by Liu et al., a short single G-quadruplex molecule was measured using the mechanically controlled break junction method (MCBJ)[69]. In this method[30,70,71], a metallic wire, usually gold, is suspended above a flexible substrate. The flexible substrate is fixed at both ends by counter supports of the substrate. A push rod is controlled by a motor or a piezoelectric actuator with vertical movement used to exert a force in the opposite direction of the counter that supports the flexible substrate. As the pushrod moves upward, the gold wire starts to break, and the distance between breakage ends can be adjusted. This study has concluded that the G-quadruplex molecule can transport high currents at relatively low bias voltages. The conductance value of the G-quadruplex is independent of the

molecule elongation. In a study by Livshits et al., a G-quadruplex molecule was measured using conductive atomic force microscopy (CAFM)[72]. G-quadruplex molecules were deposited on a mica substrate. A gold electrode was evaporated on top of the molecules using a stencil lithography technique that does not involve heat or chemical treatment. The conductive tip of the AFM gently touches the molecule, and the current is measured. This study showed that the current transported through the G-quadruplex structures up to 100 nm reaches more than 100 pA. The transport mechanism in this study occurs via long-range hopping between multi-hopping regions of the molecule.

1.6. Summary

The development of the break junction techniques contributed significantly to the advances in the understanding of the charge transport in DNA molecules. Short DNA sequences in A-, B-form were investigated heavily, and the transport properties through these molecules are understood. However, the DNA molecule also adopts other higher secondary structures. The investigation of the conductance values and the charge transport properties of these structures using the break junction technique is vital for the search of conductive molecular wires for future molecular electronics. In the proceeding chapters, the single-molecule break junction (SMBJ) technique will be used to investigate the charge transport mechanism through the G-quadruplex and DNA origami structures.

Chapter 2

DNA origami as a molecular wire

2.1. Introduction

The study and use of DNA as a building block for nanostructures have grown and evolved to address challenges in controlling and precisely positioning materials on the nanoscale level. Structural DNA nanotechnology utilizes DNA as a structural component because of its small size, predictable base-pairing interactions, and a vast range of sequence possibilities. In 1982, Nadrian Seeman proposed immobile, six-arm DNA branched junctions for building three-dimensional arrays[73]. Seeman realized that terminating the branched junctions with single-stranded overhangs may eventually base pair and lead to a three-dimensional crystalline material. Also, other forms of tile stitching DNA were recognized, such as tetrahedra[74] and octahedron[75]. The primary application for these two-dimensional DNA lattices is a bottom-up guide to orient and organize other molecules or particles on a precise scale. For example, gold nanoparticles have been organized into one and two-dimensional arrays for nanoelectronics or sensors[76].

In 2006, a different approach for building DNA structures was proposed. Paul Rothemund published a DNA folding technique that has become known as DNA origami[77]. Origami is the art known for folding a flat sheet of paper into any shaped object. DNA origami is a process of self-folding DNA. A long single DNA strand is used as a scaffold and smaller strands referred to as "staples" bridge one side of the scaffold to the other side based on the design. In 2009, Shih and coworkers achieved the construction of three-dimensional DNA origami structures[78]. Also, they developed software called caDNAno, which simplifies the design stage for sophisticated structures[79]. DNA origami is an effective process for the bottom-up fabrication of precisely well-

defined nanofeatures. Over the past decade, DNA origami has grown across multidisciplinary fields such as drug delivery[80], nanorobotics[81] and nanophotonics[82] and nanoelectronics[83].

The recent addition to the DNA origami structures' repository is the DNA nanotubes. The DNA nanotubes draw the scientists' attention in engineering because of their physical properties. Owing to the stable structure in the presence of divalent salts[84], DNA nanotubes are a potential candidate for nanowires. As previously stated, rigidity is a crucial factor in charge transport through double-stranded DNA. The DNA nanotube consists of DNAs bundled in a tube-like structure. The DNAs in the DNA nanotubes are connected via double crossover in which links between helical domains.

There are several advantages of DNA origami over the tile-stitching technique. DNA origami is an easy, one-pot process for preparing large structures. Also, DNA origami has high yields. However, the DNA origami scaffold is too long to be synthesized and usually originates from viral or plasmid genomes with known sequences. Ligation of synthetic strands or PCR amplification are techniques that have overcome the scaffold limitation.

Besides its key role as storage of genetic information in biology, DNA has also been shown to be a promising material for nanotechnology. The base recognition, self-assembly, and structural control properties of DNA are unparalleled at this size scale. Because of its rare biological, mechanical, physical, and electronic properties, DNA is a potential candidate for developing high throughput, robust and low-cost electronic devices. DNA exceptional self-assembly properties favor the bottom-up design and fabrication approach of nanoscale devices with resolutions that can surpass conventional lithographic technologies. In particular, a technique such as DNA origami has opened up the possibilities for researchers to design and build exceptionally complex nanostructures by folding long DNA strands into desired 2D or 3D shapes at nanometer scales

with high precision. DNA origami offers a step toward miniaturizing electronic devices such as high-density memory devices, which are beyond the limit of conventional silicon technology. Therefore, the study of the DNA origami properties is in the interest of science and engineering. It is predicted that the conductance may be higher than dsDNA because of the high number of overlapping pi-orbitals and its rigid structure than double-stranded DNA. In order to integrate DNA origami into a large-scale system, it is necessary to confidently and precisely investigate the charge transport through single DNA origami at smaller length scales. Moreover, an effective study of DNA origamis at smaller length scales is essential since larger DNA origamis are relatively expensive to produce.

Several reports are available for measuring the electrical resistance of metalized DNA origamis[85–87]. Metallization is a technique that has been widely studied for doping DNA origami. In this technique, DNA origami with length varies between 412 nm to 20 μm has been functionalized with gold or silver nanoparticles. However, metallization increases the cost and complexity of the fabrication process. Moreover, charge transport measurements through metalized material present a challenge to distinguish the charge pathway.

Using the single-molecule break junction (SMBJ) approach, we first examined the electrical conductance properties of 10 nm DNA origami. We then measured the conductance of a series of additional five DNA origamis that differ from the initial DNA origami by thiol location. Comparing the conductance of these six DNA origamis demonstrates that the conductance is highly insensitive to location variations of the thiol. The dominant cause for this insensitivity is that the charges are injected directly into the π-stack, and the thiols provide mechanical stability to the origami. We also examined the conductance of DNA origami at a 10 nm distance between the electrodes. We found that the conductance of DNA origami is one order of magnitude higher

than dsDNA with sequence GGC(GCTCGCC)$_3$ and indicates that DNA origami can be used as nanowires for long-range distances and can provide a template for engineering longer DNA nanowires.

2.2. Experimental procedure

2.2.1. DNA sequences

The four-helix bundle DNA origami was initially designed by Yonggang's group at Emory University (see table 2.1). The DNA origami is linked to the gold electrodes (SMBJ tip and substrate) through an alkanethiol linker which attaches to the deoxyribose ring at the 3' end.

Table 2.1: List of DNA sequences for the DNA origami

Name	Sequence (5'→3')
4hb-1-SH	ACG GCC GCG GCA GCA CGC GCG CGG CCC TGCGG[Thiol C3 S-S]
4hb-2-SH	ACT CGC ACG GCG GTC CCA ACG CCG CGT CGG TC[Thiol C3 S-S]
4hb-3	TTC CGG CCG TGC TCG ACC TCC TCT GGG ATT GTG GTT
4hb-4	TTC CGA CCG TCT GAC CGC GGT CCT AGC GAG CTC GTT
4hb-5-SH	CCG CAG GGC CGC GCG CGG ACC GCC CCA GAG GAG GTC GAG CAC GGC CGG CGA GCT CGG CGG CCG T[Thiol C3 S-S]
4hb-6	GAC CGA CGC GGC GTT GGT GCT GCC CTA GGA CCG CGG TCA GAC GGT CGG CCA CAA TCG TGC GAG T

2.2.2. DNA sample preparation and annealing protocol

The DNA strands used in this study were purchased from Biosynthesis and purified by high-performance liquid chromatography. The DNA origami under investigation here is 10 nm in length. Three sequences were purchased with a thiol linker at the 3' end (Thiol C3 S-S) see figure 2.1a. This thiol linker was protected with mercaptopropanol disulfide group during shipment and storage. Upon receipt of the strands, the oligonucleotides were suspended in distilled water (18 MΩ) for a concentration of 100 μM. These samples were then stored at -80 ºC. All measurements were carried out in a 12.5 mM Mg^{+2} buffer solution. The buffer solution was prepared with 12.5 mM magnesium acetate tetrahydrates in 1x Tris-acetate-EDTA (TAE) buffer. Before conductance measurements, 2 μL of each strand was combined with 288 μL of magnesium buffer, and the final concentration is 0.6 μM in 300 μL. Oligonucleotides were annealed to form the four-helix bundle structure by heating to 85 ºC for 10 minutes and slowly cooling the temperature from 80 ºC to 30 ºC every 2:30 minutes for each degree; then, the temperature was held at 25 ºC for 10 minutes. The sample was kept at -20 ºC until break junction experiments were performed see figure 2.1b.
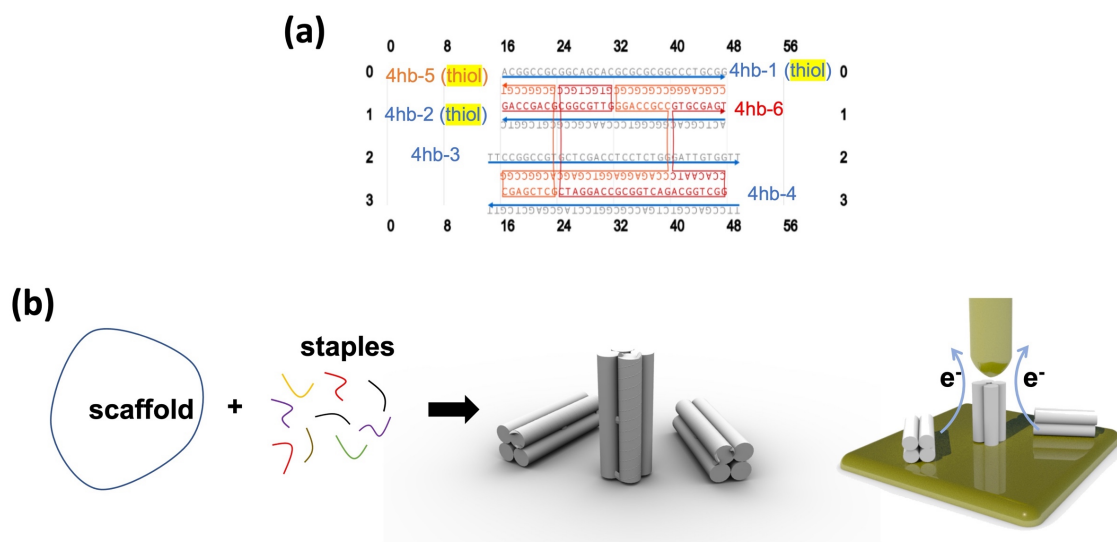
Figure2.1: (a) the DNA sequences from caDNAno showing the thiols locations. (b) schematic representation of the experimental procedure from annealing the DNA strands to SMBJ.

2.3. Results and discussion

2.3.1. DNA origami structure study and melting temperature

Circular dichroism (CD) spectra are one of the primary methods for understanding the structure of nucleic acids. Figure 2.2a shows the CD spectra of the DNA origami at different temperature values. The spectrum of the DNA origami exhibits similar features as B-form dsDNA; both spectra have a positive peak at 280 nm and shallow negative peaks at 210 nm and 250 nm[53]. High humidity favors the B-form DNA. In addition, we estimated the melting temperature of the DNA origami to be 70 °C. This suggests that the DNA origami structure is stable at room temperature see figure 2.2b. However, DNA origami is not fully unfolded; this is seen as the CD spectrum at 95 °C was acquired, which is probably due to the high GC content in the sequence.

(a)

(b)
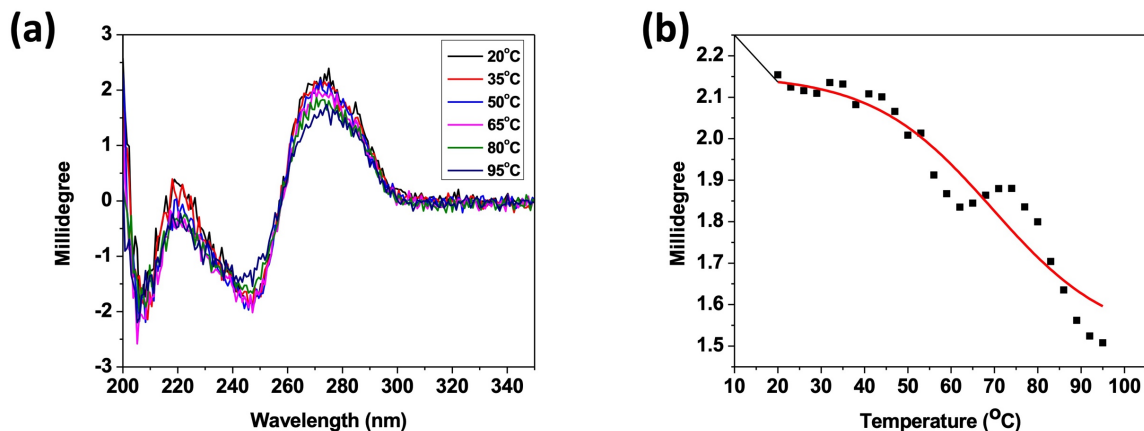
Figure2.2: (a) CD spectra of the DNA origami at different temperature values. (b) The melting temperature of the DNA origami is obtained from the CD spectra at 280 nm. The red line represents a sigmoidal fitting to the experimental data.

2.3.2. Conductance measurements

2.3.2.1. SMBJ tapping mode

The DNA origami was modified with three thiol linkers, and there are additional thymine basses that offer binding sites to gold. The DNA strands were hybridized in one tube. Conductance measurements were conducted by bringing an atomically sharp gold tip coated with Apiezon wax to minimize the ionic leakage current below ~1 pA into and out of contact with a gold substrate with the DNA origami in solution. A schematic representation of the SMBJ is shown in Figure 2.3a. Current traces were monitored as the tip was retracted away from the substrate. When DNA origami bridges the gap between the tip and the substrate, a step in the current trace appears see figure 2.3b. In the absence of the molecule, current traces show no features see figure 2.3c. By collecting thousands of current traces, one can perform a statistical analysis of these traces, which yields a histogram with the most probable conductance of a DNA origami see the black histogram in figure 2.3d. The high number of counts between $1x10^{-6}$ G_0 and $1x10^{-4}$ G_0 is due to the poor

insulation of the tip, which leads to an increase in the ionic leakage current. Multiple independent conductance measurements fitted with a Gaussian distribution yielded a conductance value of $3.6 \times 10^{-3} G_0$ for this DNA origami. In contrast, when no molecules are present, conductance histograms yield no peak (see figure 2.3d red histogram).
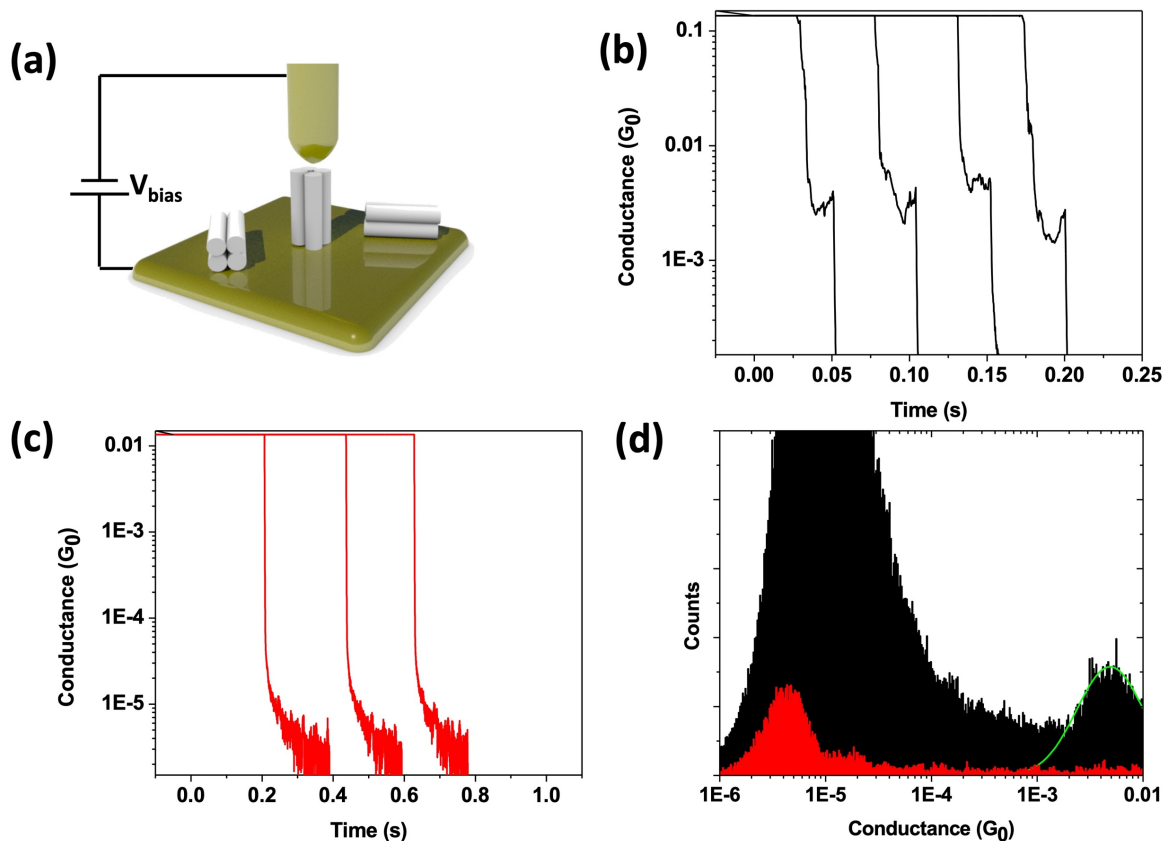
Figure2.3: (a) schematic representation of the SMBJ experimental set-up showing the DNA origami molecule bridging the gap between the two electrodes. (b) representative conductance traces vs. time showing steps when the molecule binds to both electrodes. (c) traces when no molecule binds. All traces in (b) and (c) are offset horizontally for clarity. (d) Conductance histograms for the DNA origami (black histogram) and only buffer (red histogram). A total of 5000 traces were obtained for each sample.

2.3.2.2.   SMBJ flyfishing mode

Another SMBJ mode is introduced to examine the conductance of the DNA origami as the gap between the gold tip and substrate is equal to the DNA origami length. This mode is referred to as flyfishing mode. The tip is brought to a distance ~1.6 nm away from the substrate and it is considered to be the starting point. Then, the tip is retracted below the minimum current setpoint ~ 10 nm, and the current traces are recorded (see figure 2.4a). This mode makes sure that the tip picks up a molecule and stretches it. Additional substrate surface treatment was used to help orient the DNA origami normal to the surface. Here, we used 6-Mercapto-1-hexanol (MCH) molecules after DNA deposition to improve the SAM formation. The sequence used in this experiment is shown in figure 2.1a. A single trace of the flyfishing mode is shown in figure2.4b; as the distance between the gold tip and the substrate increases, the conductance value is relatively high before the conductance drops suddenly, indicating the gold thiol breakage. However, the tip at this point may never reach the minimum value, so it keeps retracting until the current drops below the minimum current setpoint. This process was repeated thousands of times, and the results were processed manually. As shown in figure 2.4c, there are multiple traces with conductance values between $3.16 \times 10^{-3} G_0$ and $5.62 \times 10^{-3} G_0$ at distances greater than 8 nm. Here we conclude that the DNA origami with 10 nm length has a high conductance value, possibly due to the molecule's rigidity, which makes the π-stack stable.
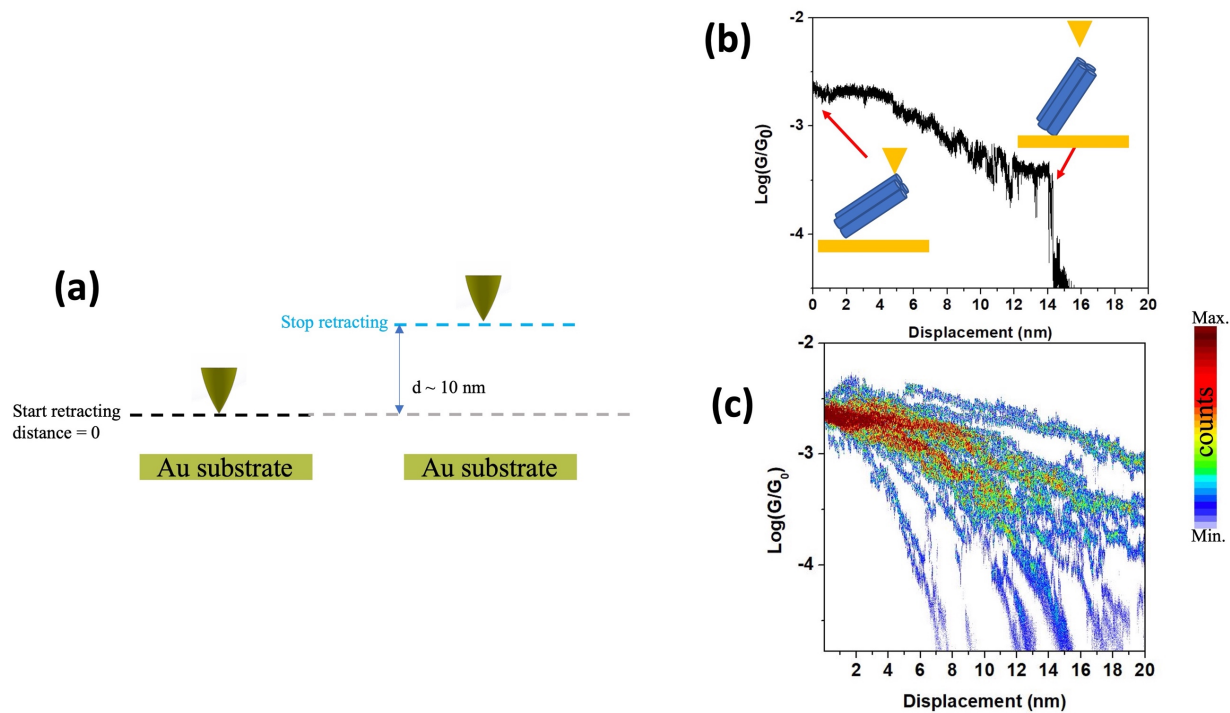
Figure2.4: (a) illustration of the flyfishing mode. (b) single trace of the conductance vs. distance. (c) 2D histograms of the flyfishing traces.

2.3.3. Thiols effect on the DNA origami conductance value

Control experiments to ensure the conductance value measured is due to the DNA origami were performed. Figure 2.5 shows the conductance histogram of the original DNA origami where the thiols are protected with mercaptopropanol disulfide group. There is no peak in the histogram, which suggests no molecule bridging the gold electrodes. Moreover, conductance histograms of the DNA origami with one or two thiols on one side show similar results for the thiols protected state see figure 2.6.
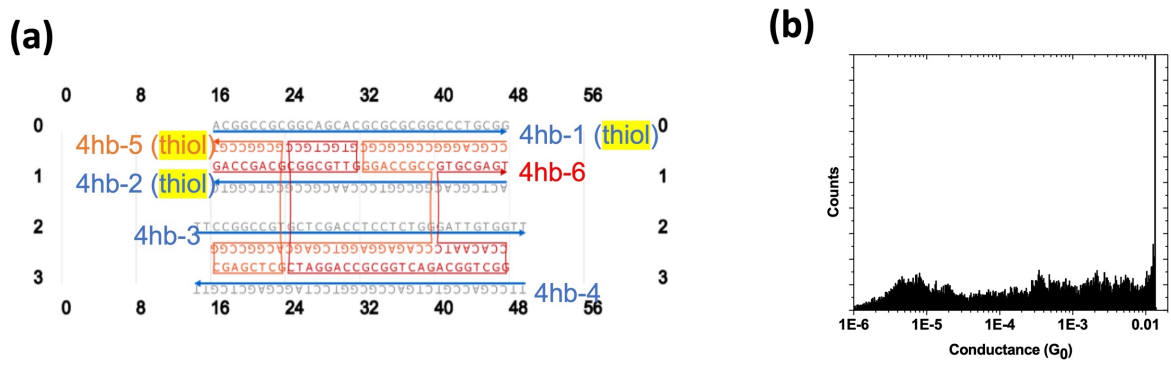
Figure2.5: (a) the DNA origami sequence and the thiol locations used in this control experiment. (b) the conductance histogram reveals no peak for the molecule where the thiols are protected with mercaptopropanol disulfide group.
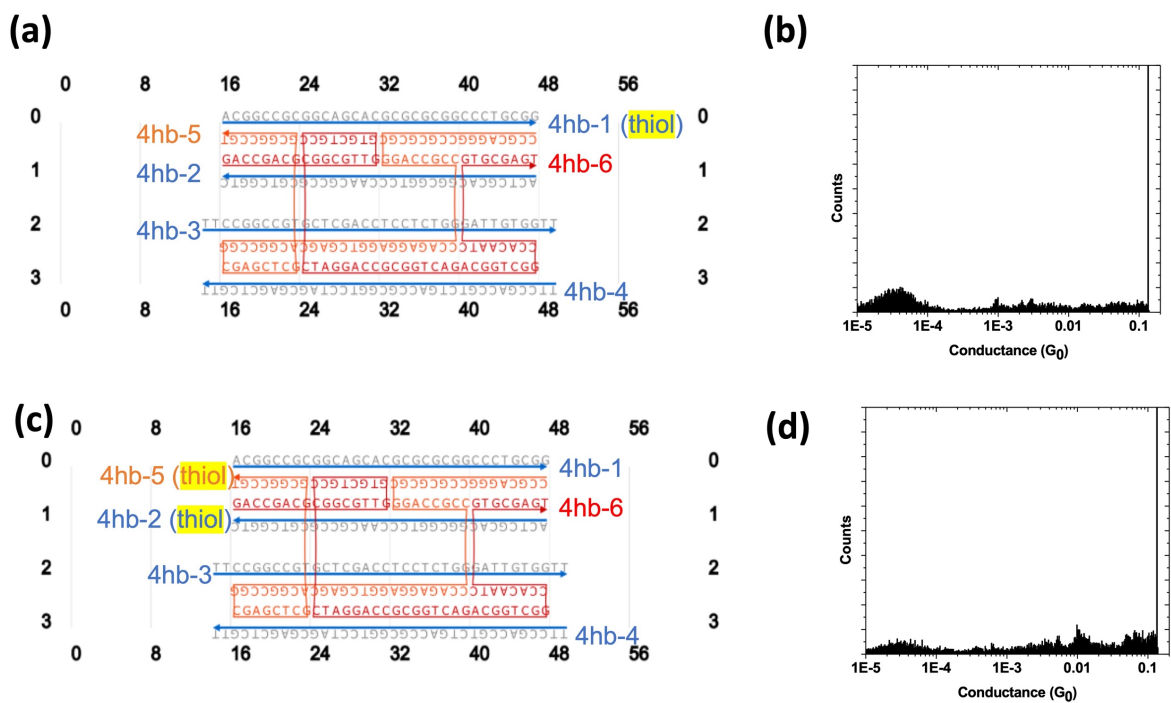
Figure2.6: (a) and (c) show the DNA origami sequence and the thiol locations used in this control experiment. (b) and (d) present the conductance histograms for the control experiment where no peak appears for the molecule.

Next, we examined the effect of contact location on the DNA origami conductance value. We measured several DNA origamis with sequences that differed from our original design by only the thiol attachments. By changing the thiol locations on the DNA origami, it allows charges to take different routes. Also, we replaced 4hb-3 and 4hb-4 strands with similar sequences except for the thymine bases at the end see figure 2.7a. The means of the gaussian fittings of the conductance peaks were plotted against the thiol locations on the DNA origami are shown in figure 2.7b. The conductance value is less sensitive to the thiol locations, and the thiols provide stability to the molecule by chemically binding the molecule to the gold electrodes.
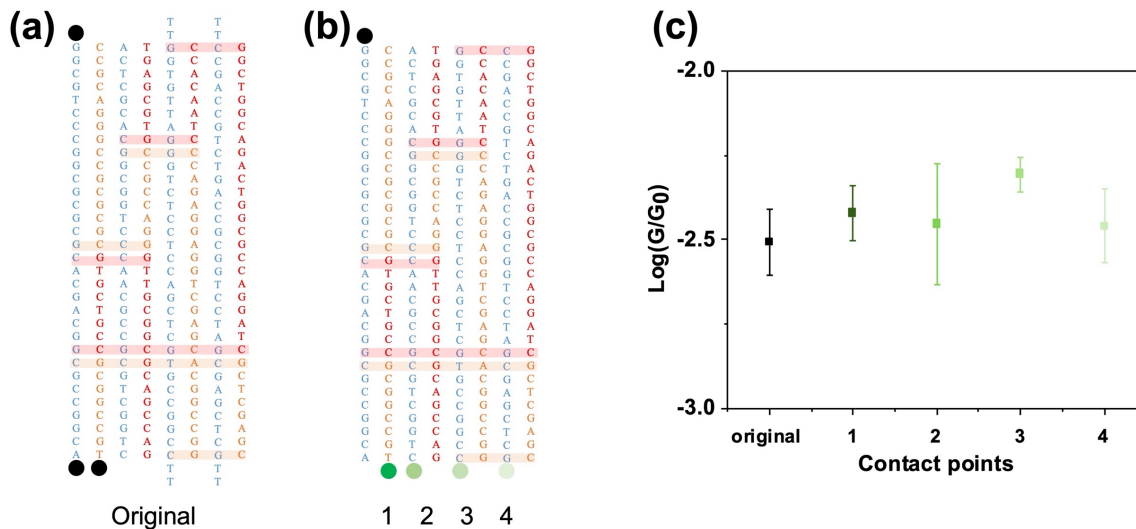
Figure2.7: (a) Representative the original DNA origami sequence with black circles are the thiol locations. (b) the thiol locations vary from 1 to 4 while the thiol on the other side of the molecule is fixed. (c) the conductance value obtained from the mean of the Gaussian fitting of the peak in the conductance histogram, and the x-axis is the thiol locations on the DNA origami. Error bars are the slandered deviation of the mean with N = 3.

2.4. Summary

In this work, we examined the structure of the DNA origami using the CD spectra. The molecule is partially melted at 70 ºC. The CD spectra at 95 ºC suggest unfolded molecule, which is due to the high guanine and cytosine content. SMBJ measurements showed that the conductance of long single DNA origami could be measured. We have found that the conductance value is high compared to dsDNA with a similar length. Control experiments were conducted on the molecule to ensure no contaminations or other factors that contributed to the peaks in the conductance histograms. The thiols have less impact on the charge pathway as it provides mechanical stability to the molecule during the measurements. This finding was concluded from the experiment where the thiols were placed in different locations on the DNA origami. These findings may enable the fabrication of DNA-based nanoelectronics devices where the DNA origami is used as a connector. Further studies are required to scrutinize the charge transport mechanism in DNA origami structures, such as length or temperature dependence.

Chapter 3

Charge transport in G-quadruplexes

3.1. Introduction

Deoxyribonucleic acid (DNA) serves as a potential functional element in solid-state molecular electronics because of its unique self-assembly properties, which superbly exceed conventional lithographic technologies in terms of resolution. In recent decades, copious studies have been published on the interplay between electronic property in double-stranded DNA (dsDNA) and length, sequence, environment, ribonucleic acid (RNA), or conformation. Moreover, research has expanded to non-canonical DNA structures such as guanine-quadruplexes (G-quadruplex).

Guanine-rich DNA molecules form stable quadruplex structures by stacking several planes of four guanine bases (G-tetrad) associated via Hoogsteen hydrogen bonding[88]. DNA guanine-rich strand folds with the aid of univalent ions from one or multiple strands into parallel or antiparallel conformations depending on the orientation of the strands in a G-quadruplex. There are numerous factors that govern the topology of the G-quadruplex, such as ions, sequence, and loop length. Despite the potential role of DNA G-quadruplexes in regulating multiple biological processes[89], G-quadruplex continues to attract attention as a promising building material for nanotechnology[90]. Several theoretical studies have proposed that DNA G-quadruplex structures efficiently transport charges over long distances due to their less-flexible structure and higher number of overlapping π electrons between guanine planes[91,92].

Although systematic and direct contact conductance measurements in aqueous solution have not been conducted on G-quadruplexes, multiple experimental studies have been employed to examine the charge transport mechanisms using either photochemical[93,94] or electrical measurements[69,72]. These measurements suggest that the charge transport in G-quadruplex systems is possible, and

the charge transfer rate was observed to be weakly length-dependent, indicating a hopping mechanism.

In this work, we present a systematic study of the charge transport properties of the G-quadruplex systems in a sodium phosphate buffer solution at the single-molecule level to understand the charge transport mechanism. We use circular dichroism (CD) spectroscopy to investigate the conformation of series molecules $G_nT_3G_n$ with n = 3-5 and find that all molecules adopt the G-quadruplex structure with antiparallel topology. We employ the single-molecule break junction (SMBJ) approach to obtain the conductance values for the series of G-quadruplex molecules and extract their length-dependent exponential decay constant β-value. We find that the resulting length-dependent conductance data suggest a sequential hopping charge transport mechanism.

3.2. Experimental procedure

3.2.1. Sample preparation

The oligonucleotides investigated here were purchased from Biosynthesis, IDT, and Alpha DNA. The DNA molecules were purified by high-performance liquid chromatography (HPLC). The 3' end of the oligonucleotides were modified with thiol linkers via a three-carbon spacer. All DNA strands were stored at -80ºC. Prior to measurements, the tris(2-carboxy-ethyl)phosphane (TCEP, 12.5mM) was used to reduce the disulfide bond in the thiolated strands for 3 hours at room temperature. Then, the excess and unreacted TCEP was removed using 7k molecular-weight cutoff desalting spin columns (ThermoFisher scientific Zeba # 89882). All experiments were conducted in 100mM phosphate buffer (PB). The 100mM PB was prepared by adding Na_2HPO_4 and NaH_2PO_4 (Sigma-Aldrich) in a ratio of 8.1/1.9 to obtain a 7.4pH solution. All solutions were

prepared using Milli-Q water (18MΩ). Hybridization was obtained by heating the mixture to 90ºC and then cooling it to 23ºC at a rate of 1ºC/minute. Then, the mixture was stored at -20ºC.

3.3. Results and Discussion

3.3.1. Length dependence study of G-quadruplex conductance

We conducted break-junction measurements on the series of DNA G-quadruplexes $G_nT_3G_n$ with n = 3-5 (see figure 3.1a). We modify the 3' ends of the DNA strands with thiol linkers to ensure a good binding between the G-quadruplex and the gold electrodes used in the SMBJ. Figure 3.1a illustrates a schematic of the measurement's setup; a thiolated three stacked G-quadruplex with sequence $G_3T_3G_3$ is linked between the gold tip and substrate. Single-molecule break junction measurements involve an atomically sharp tip that approaches the substrate surface until the current amplifier is saturated. Then, the tip is retracted at a rate of 80 nm/s while the current is recorded until the current reaches the resolution of the amplifier. This process is repeated to collect thousands of individual current traces for statistical analysis. A step in the current trace (see figure 3.1b) indicates a molecule is bridging the gap between the tip and substrate. Individual traces that meet the selection criteria are automatically added to a conductance histogram using a laboratory-developed LabVIEW program (figure 3.1c). Accumulation of steps in the conductance histogram results in a peak that represents the most probable conductance for a single-molecule junction. Additional control experiments performed with non-functionalized DNA strands do not show steps in this conductance range (see figure 3.1c).
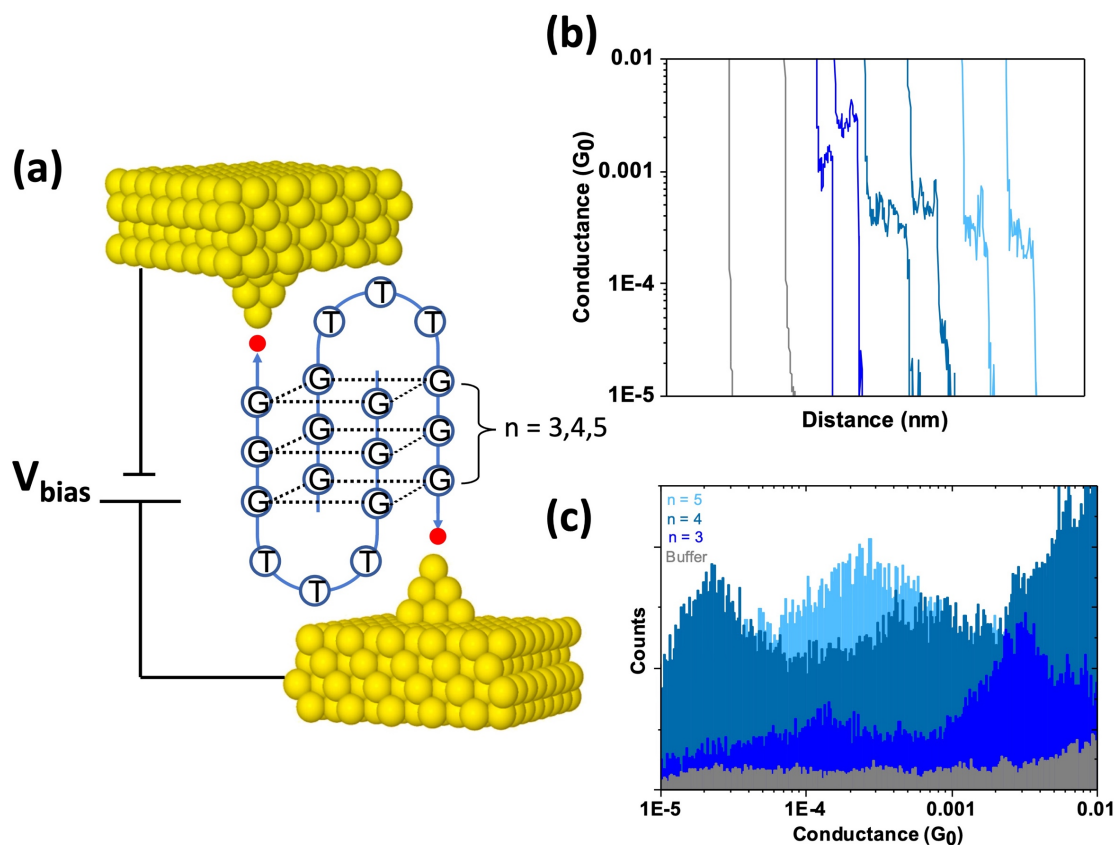
Figure3.1: (a) idealized SMBJ set-up with G-quadruplex molecule bridging the electrodes. Red dots represent the thiol linkers. (b) conductance vs. distance traces showing step features (Cayan for n = 5, navy for n= 4, and dark blue for n = 3). Gray traces for buffer only and exhibit no step features. (c) conductance histograms for buffer only (gray histogram) and G-quadruplexes n = 3,4,5.

In order to understand the charge transport properties in the G-quadruplex system, it is essential to explore the length dependence of the conductance. Therefore, we performed SMBJ measurements on a series of G-quadruplexes with sequences $G_nT_3G_n$ where n = 3-5. Figure 3.2 shows the conductance value decreases as the number of guanines increases. It is possible to obtain β value, which is often used as a figure of merit to provide insights into the charge transport properties of the system by plotting the natural logarithmic of the conductance versus G-quadruplex length. We

obtain β value of 0.38Å^{-1} for the G-quadruplex system, and this value is within the range of a hopping transport mechanism.
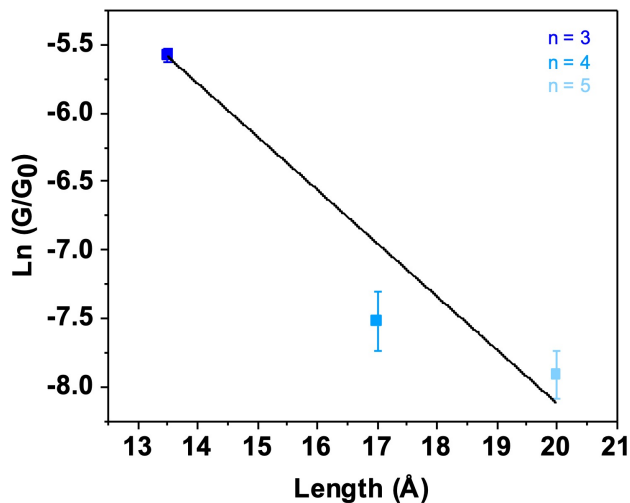
Figure3.2: natural logarithm of conductance values versus length for the G-quadruplex structures. The solid black line is linear fitting that gives ß = 0.38Å^{-1}. Error bars are slandard errors of the mean for a sample size of 3 for each G-quad.

3.3.2. G-quadruplex topology and melting temperature study

We performed circular dichroism (CD) measurements at room temperature to ensure that the DNA sequences in this study form G-quadruplex with an antiparallel topology which indicates that the thiols are in opposite directions for binding to the gold electrodes. The CD spectra of the $G_nT_3G_n$ where n = 3-5 shows a clear positive peak at a wavelength of 295 nm, indicating the antiparallel G-quad structure (see figure 3.3). There are many antiparallel conformations that the CD cannot discriminate. The primary source of distinct CD spectra is the polarity of the tetrads. The polarity here is referred to as the guanine glycosidic anti/syn conformations. All antiparallel or parallel G-quadruplex possess similar tetrads polarity. Therefore, NMR or X-ray crystallography experiment

is required to determine the topology of the G-quadruplex. Fortunately, G-quadruplex with n = 4 has been investigated with NMR and X-ray, and the exact structure is formed by dimerization of two hairpins with lateral loop[95]. To determine the stability of the G-quadruplex structures, we examined the melting temperature of the G-quadruplex. Figure3.3b shows the intensity of the peak at 294 nm as a function of temperature. As the temperature increases, the G-quadruplex structure starts to unfold, and the peak intensity drops. Fitting the data with sigmoidal function (solid lines in figure 3.3b), we extracted a melting temperature of the G-quadruplex structures. The extracted melting temperatures are listed in Table 3-1. All three G-quadruplexes have a melting temperature higher than the room temperature by more than 15ºC, which indicates that the G-quadruplex structure studied is in a stable antiparallel form.
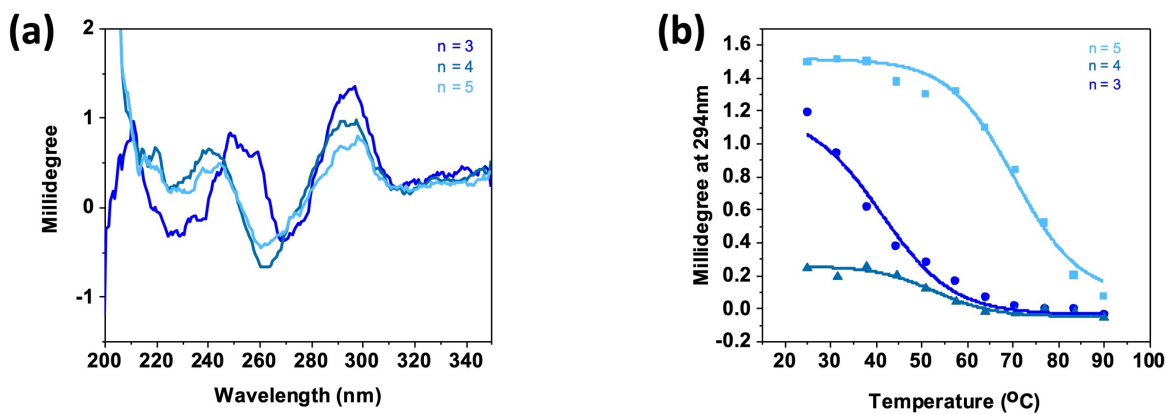
Figure3.3: (a) Circular dichroism spectra of the G-quadruplex with n =3,4 and 5. (b) melting temperature curves for all g-quadruplexes. The solid line represents the sigmoidal fitting to the experimental data. All measurements were conducted in 100mM sodium phosphate buffer with pH=7.3.

Table3.1: melting temperature values extracted from the sigmoidal fitting to the experimental data

n (G_nTTTG_n)	3	4	5
Melting Temperature (ºC)	41.22	53.02	70.39

3.4. Theoretical discussion

Single-molecule electrical and photochemical experiments examining charge transfer in G-quadruplex structure resulted in a weak length dependent[72,96]. These results were explained by thermally activated hopping between multi-quartets of the G-quadruplex. This work also suggests a weak length dependence through the G-quadruplex structures, which indicates a thermally-activated hopping charge transport mechanism.

3.4.1. Hopping model

To verify that the hopping model dominates the charge transport mechanism in G-quadruplex structures, we start with the simplest hopping model, which treats each guanine as an independent hopping site. Therefore, the predicted resistance is proportional to the number of hopping sites. Figure3.4 shows the resistance of the G-quadruplex molecules versus the number of G-quartets and a fitting of the experimental data with a linear hopping model (dashed line). The coefficient of determination (R^2-value) for the linear fitting is 0.98, indicating that the hopping model can explain the data.
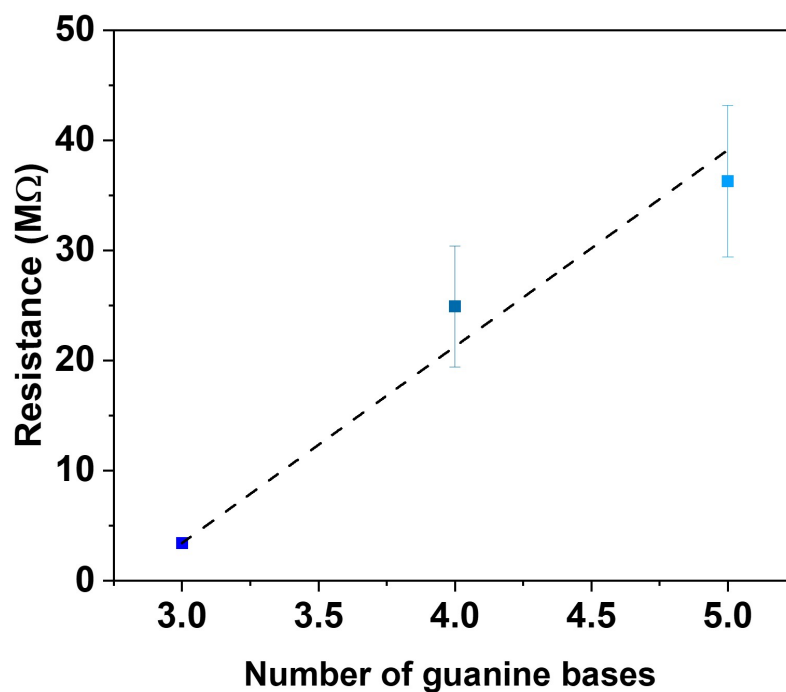
Figure3.4: The resistance of the G-quadruplex plotted versus the number of guanines. The dashed line is the linear fitting. Error bars are the standard error of the mean with sample size N = 3.

3.5. Summary

These results demonstrated that the G-quadruplex structures in sodium phosphate buffer solution are formed by two hairpins, and the molecules are stable at room temperature. The charge transport in these structures can be described with the hopping model, in which each guanine base is a hopping site. In contrast to double-stranded DNA, charge transport mechanisms in short and long G-quadruplex structures follow the hopping model

Chapter 4

Identification of DNA structural conformation via single-molecule conductance

4.1. Introduction

Miniaturization of electronic devices has long been pursued in many interdisciplinary fields of nanotechnology[97–100]. Deoxyribonucleic acid (DNA) has always been the subject of interest in nanoelectronics because of its exceptional self-assembly properties, which enables a unique approach for bottom-up fabrication nanodevices with unparalleled resolution at nanoscale[77]. Future molecular electronics, which incorporates molecules as a functional element, draw considerable attention to understanding the charge transport in double-stranded DNA (dsDNA)[101]. Theoretical studies of charge transport in DNA suggested undisturbed and compacted π-orbital will result in high DNA conductance[102]. Therefore, relatively rigid DNA structures such as guanine-quadruplex (G-quadruplex) have been studied for potential roles in nanoelectronics.

DNA sequences rich in guanine bases can form in the presence of counter ions stable four-stranded structures, which are made up of stacking planes of four guanines held together by eight hydrogen bonding[61]. Circular dichroism (CD) is one of the primary methods for understanding the structure and topology of G-quadruplexes[61,103]. In general, depending on the sequence, loop length, and univalent ions, the strand directions in G-quadruplex topology can be parallel, antiparallel, or hybrid (3+1)[104]. Also, G-quadruplex could be formed with a single strand (intramolecular) or multi-strands (intermolecular). However, CD spectra interpretation may be misleading when DNA duplexes and G-quadruplexes coexist for self-complementary guanine-rich DNA sequences. Recently, the single-molecule break junction (SMBJ) technique has arisen as a promising tool in

measuring single-molecule conductance value for various DNA and RNA sequences[105], conformations[106], environmental effect[107], and base mismatches[108]. In this article, we present the use of electrical conductance measurements using the SMBJ technique as a sensing platform of G-quadruplex in conjunction with CD spectra to detect and identify different DNA conformations.

4.2. Experimental procedure

4.2.1. DNA sample preparation

The oligonucleotides investigated here were purchased from Biosynthesis, IDT, and Alpha DNA. The DNA molecules were purified by high-performance liquid chromatography (HPLC). The 3' end of the oligonucleotides were modified with thiol linkers via a spacer (six-carbon chain for M1 and a three-carbon chain for M2). All DNA strands were stored at -80 ºC. Prior to measurements, the tris(2-carboxy-ethyl)phosphane (TCEP, 12.5mM) was used to reduce the disulfide bond in the thiolated strands for 3 hours at room temperature. Then, the excess and unreacted TCEP was removed using 7k molecular-weight cutoff desalting spin columns (ThermoFisher scientific Zeba # 89882). All experiments were conducted in 100mM phosphate buffer (PB) and 100mM potassium chloride (KCl). The 100mM PB was prepared by adding Na_2HPO_4 and NaH_2PO_4 (Sigma-Aldrich) in a ratio of 8.1/1.9 to obtain a 7.4 pH solution. For the 100 mM KCl, the solution was prepared by adding 15 mg of KCl to 100mM PB to get a solution with a 7.3 pH level. All solutions were prepared using Milli-Q water (18 MΩ). Hybridization was obtained by heating the mixture to 90 ºC and then cooling it to 23 ºC at a rate of 1 ºC/minute. Then, the mixture was stored at -20 ºC.

4.2.2. CD experiment set-up

CD measurements were conducted using an Olis RSM 1000 circular dichrometer with a cylindrical cell (170μL) with 0.1mm path length. A baseline spectrum of buffer only was collected before adding the DNA. Non-thiolated hybrids were prepared using the above-mentioned annealing protocol. A 170μM of solution with 25μM DNA concentration was added to the cylindrical cell.

4.3. Results and discussion

4.3.1. SMBJ conductance results

We performed single-molecule break junction (SMBJ) conductance measurements on self-complementary and double-stranded DNA sequences. The 3' end of the DNA strands were modified with thiol linkers via spacers to ensure a binding between the DNA hybrid and the gold electrodes used in SMBJ (figure 4.1a). The sequences in this study are M1: $(GC_3)_3$ and M2: $(C_3G_3)_2$. A schematic illustration of the SMBJ with 12 base pairs dsDNA attached between the gold tip and the gold substrate is shown in figure 4.1b. SMBJ measurements were conducted by bringing the gold tip into and out of contact with the gold substrate with the DNA hybrids in the solution. Current traces were recorded and monitored as the tip retracted, and steps in the current versus distance traces suggest the formation of Au-DNA-Au junctions figure 4.1c. With thousands of rapidly collected individual current traces, a statistical analysis of these traces yielded a histogram that exhibited two apparent peaks for both DNA molecules figure 4.1d. The lower conductance values for both sequences are 1.5×10^{-4} G_0 and 2.5×10^{-4} G_0 for M1 and M2, respectively, which are within the range of previously reported short GC-rich dsDNA (B-form)[53,109]. Several control experiments conducted in 100 mM PB such as no DNA in the solution,

single-stranded DNA, and unreduced thiols on the DNA strands imply that these peaks mainly were contributed to DNA molecules, rather than other factors such as counterions, water molecules in the solution, or single-stranded DNA see figure 4.2. The complementary sequence of M1 (Rseq1) and the self-complementary M2 has three consecutive guanines, which may form G-quadruplex beside the double-stranded DNA (dsDNA)[110].
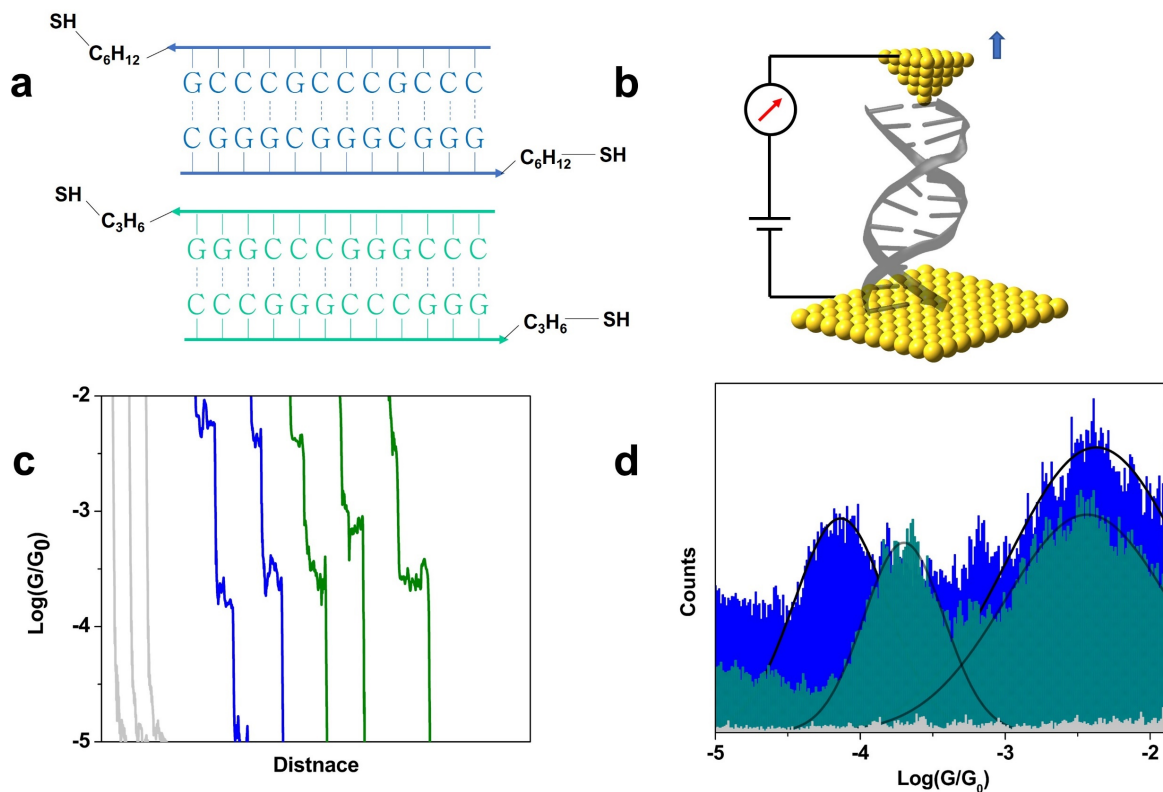
Figure 4.1: (a) schematic of the examined DNA sequences. The 3' represented by an arrowhead shows the thiol linkers. (b) Simplified schematic of the experimental setup showing the dsDNA bridged between two gold electrodes. (c) Multiple single-molecule conductance vs. distance traces at room temperature. The gray traces demonstrate when no molecule bind to the electrodes, and the blue and green for M1 and M2 when binding to electrodes, respectively.

All traces were offset horizontally for clarity. (d) conductance histograms for two DNA hybrids and control experiment for blank buffer.
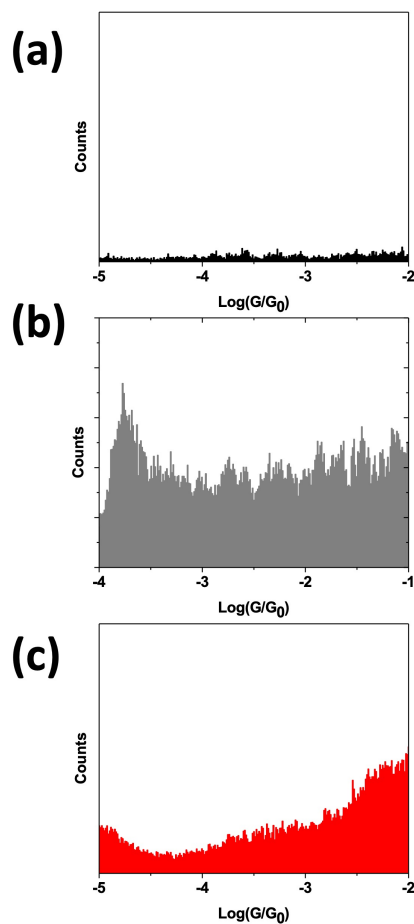
Figure 4.2: Control experiments (a) 100mM sodium phosphate buffer (PB). (b) single stranded DNA M1 in 100mM PB buffer. (c) dsDNA M2 in 100mM PB and the thiols are in the unreduced form.

4.3.2. CD structure and melting temperature study

To examine the effects of structure on charge transport, we performed circular dichroism (CD) measurements. CD spectra provide an insight on the DNA conformations by measuring the absorbance difference between right and left circularly polarized light[50]. Because single-stranded

52

Rseq1 is not a self-complementary sequence, Rseq1 is a control sequence for M2. The CD spectra of M1, M2, and Rseq1 are shown in figure 4.3. M1 and M2 CD spectra indicate the formation of multiple conformations in the solution. The CD may suggest the formation of B-form and a G-quadruplex in the solution[50,61]. dsDNA M1 CD spectrum exhibit a positive shoulder-like peak at 295 nm, a positive peak at 260 nm, and two negative peaks at 240 nm and 210 nm. It is almost impossible to empirically determine the structure of the DNA from such a CD spectrum.

On the other hand, Rseq1 adopts antiparallel topology of the G-quadruplex, which is identified by the presence of the 295 nm, 210 nm, and 260 nm positive peaks. The self-complementary M2 shows a negative minimum of around 280 nm. There is an ambiguity in the spectra that are not fully understood.

Figure 4.3. CD spectra of the two DNA hybrids (blue and green) (a) and (b). Single-stranded Rseq1 (light blue). CD measurements were conducted at room temperature and in 100mM PB.

Another helpful tool that may identify how many structures are available in a DNA solution based on the size of the structure is Gel electrophoresis. The Gel measurements are shown in figure 4.4. The dsDNA of M1 and M2 reveal one band close to the size of 12bp. However, the single-stranded M1 Rseq shows two bands; one is slightly below 20bp, and the second is around 12bp. These results suggest that Gel electrophoresis detected one band for the dsDNA M1 and M2, probably the B-form, and two bands for the M1 Rseq are for G-quadruplex and unfolded single-stranded,

respectively. Unfortunately, gel electrophoresis and CD experiments could not detect the two structures for the dsDNA M1 and M2.
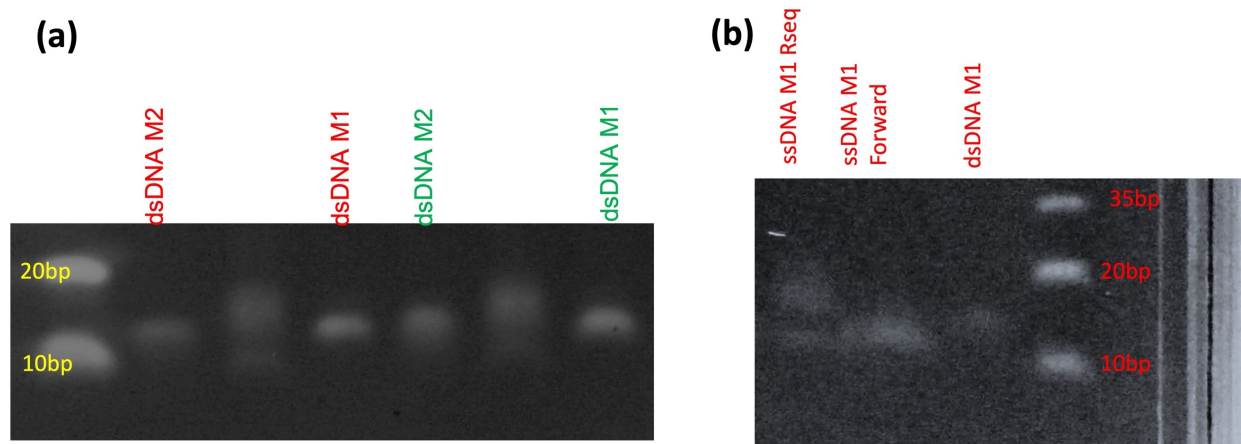
Figure4.4: Gel electrophoresis conducted in 100mM PB with a concentration is approximately 2uM. (a) results for dsDNA M1 and M2. (b) single-stranded M1 reverse sequence (Rseq) and forward sequence with dsDNA M1.

Another approach that may identify two formations in a DNA solution is the melting temperature measurements of the molecules. The melting temperature is defined as the temperature where the DNA strands are 50% in a single-stranded form. Hypothetically, the unfolding process of two different structures occurs at different temperatures depending on the number of hydrogen bonds. For example, DNA with a higher number of hydrogen bonds has a higher melting temperature than DNA with a lower number of hydrogen bonds. Figure 4.5 plots the absorbance intensity at 260 nm as a function temperature. The intensity of dsDNA is lower compared to ssDNA, and the absorbance increases as a function of temperature. The melting temperatures for all sequences obtained from the absorbance vs. temperature fittings and from the Integrated DNA Technology (IDT) oligo analyzer tool are listed in table 4-1. The difference in values between the measured and calculated is insignificant. However, the melting temperature curve of the dsDNA M1 shows two unfolding processes. This probably is due to the presence of two different DNA structures.

Therefore, CD, Gel electrophoresis, and melting temperature experiments suggest a secondary structure in the dsDNA solution.
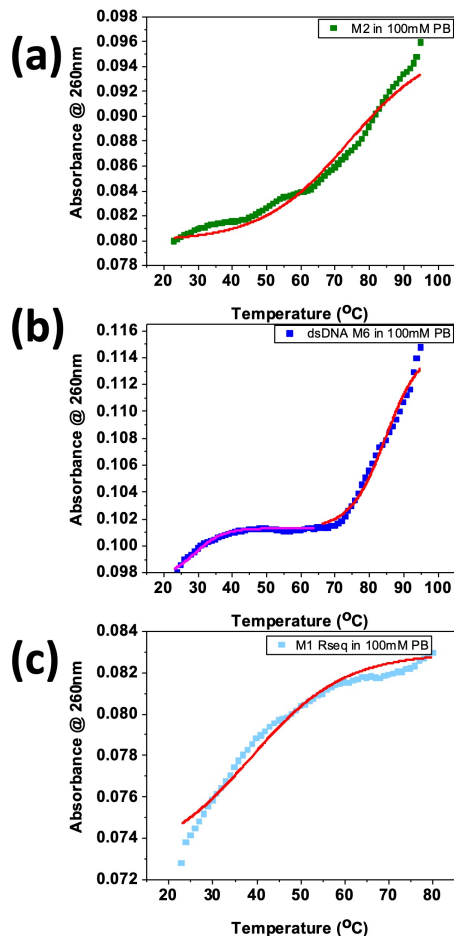
Figure4.5: Absorbance vs. temperature measurements for (a) dsDNA M2. (b) dsDNA M1 and (c) Rseq M1. All measurements were conducted with a 0.1mm quartz cuvette. Solid lines are the sigmoidal fitting of the experimental data.

Table 4.1: Melting temperature values estimated from UV absorbance measurements and calculated values from IDT oligo analyzer tool.

	Measured T_m (ºC)	Calculated T_m (ºC) from IDT
dsDNA M1: $(GC_3)_4$	29.3ºC and 85.83ºC	82.5ºC
Rseq M1: $(G_3C)_4$	38.6ºC	Not available

dsDNA M2: $(G_3C_3)_2$	74.17 ºC	79.9 ºC

4.3.3. The effect of potassium ions on the DNA G-quadruplex conformations

The above two sections discuss the possibility of two structures in the dsDNA solution. The second structure may be G-quadruplex in the antiparallel form. Many thermodynamic studies of the oligonucleotides revealed that potassium ions destabilize the antiparallel topology and favor the parallel topology[62,111]. This is probably due to the bigger size of the potassium, which forces the guanines to adopt certain orientation. Here, the addition of K+ ions significantly changed the CD spectrum for Rseq1 to a parallel conformation see figure 4.6c. Also, a slight change to the CD spectra for both M1 and M2 hybrids at the 295 nm wavelength. Although CD spectra are one of the primary methods for understanding the structure of DNA hybrids, the CD spectra of M1 and M2 are not conclusive. In contrast to parallel topology, the thiols bind to both SMBJ electrodes while the G-quadruplex adopts the antiparallel topology. SMBJ technique may identify the structure based on the electrical conductance of the junction.
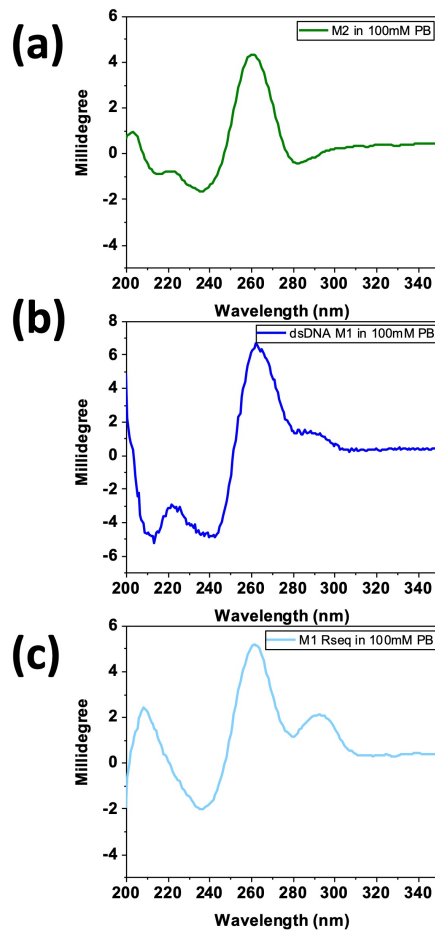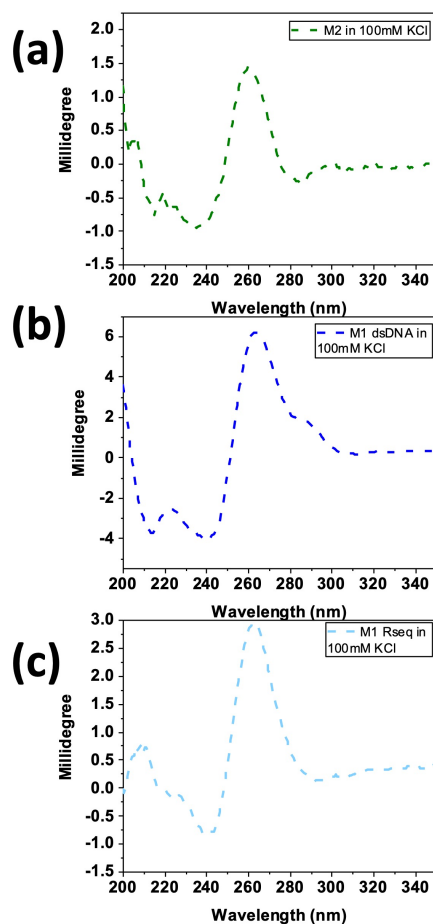
Figure 4.6: CD spectra of the two DNA hybrids (dashed blue and green) (a) and (b). (c)Single-stranded Rseq1 (light blue). CD measurements were conducted at room temperature and in 100mM PB + 100mM KCl.

SMBJ measurements on Rseq1 in 100mM KCl show no significant plateaus in the current traces, which yielded no peak in the conductance histogram. Because all thiols were in the same direction in the presence of potassium ions, stable Au-G-quad-Au junctions were not possible. The conductance histograms obtained for M1 and M2 in 100mM KCl solution show one conductance

peak (figure 4.7, green histograms). The conductance values are -3.54±0.14 and -3.47±0.04 for M1 and M2, respectively. These values are similar to what was obtained for M1 and M2 in 100mM PB, which is probably the conductance value for B-form DNAs.
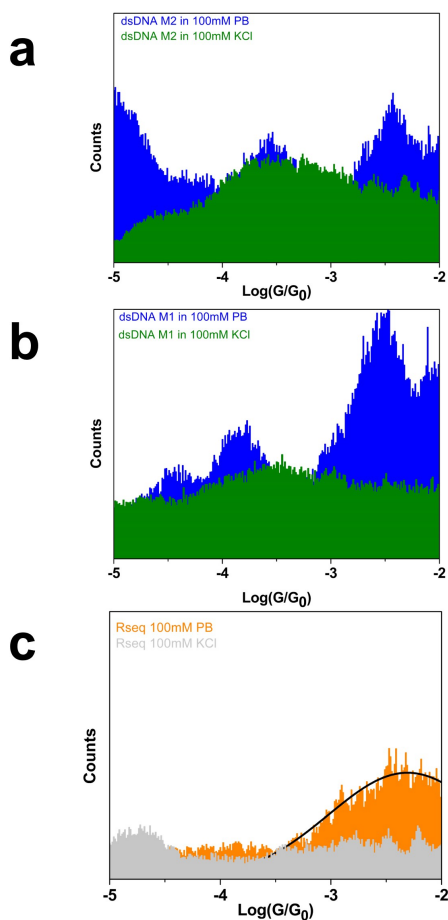
Figure 4.7: Conductance histograms for DNA hybrids (a) M2 measured in 100mM PB (blue) and 100mM KCl (green). (b) M1 conducted in 100mM PB (blue) and 100mM KCl (green). (c) thermally annealed single stranded Rseq1 in 100mM PB (orange) and 100mM KCl (gray).

4.4. Summary

In this work, we have studied the conductance of DNA sequences with three consecutive guanines. While M1 and Rseq1 form hybrid, M2 is a self-complementary DNA. We found two conductance values for M1 and M2 and attributed them to two DNA conformations present in 100mM PB. Different experiments, including CD, Gel electrophoresis, and melting temperature, lack the advantage of single-molecule detection. The effect of potassium ions on G-quadruplex conformations allows the SMBJ to detect antiparallel structures. However, there are certain limitations as well. The G-quadruplex structure must be labeled with thiols for binding with gold electrodes. Also, SMBJ will measure the conductance of G-quadruplex only if the thiols are at both ends of the G-quadruplex. The effect observed here can be relevant for the design of nanodevices that detects the electrical signal for different DNA conformational differences in a solution.

Chapter 5

Conclusion and outlook

5.1. Conclusion

Over the past two decades, DNA and ribonucleic acid (RNA) molecules have been extensively studied using the scanning tunneling microscopy-break junction technique for their potential role in molecular electronics. The understanding of molecular-scale transport on unique DNA structures is one of the fundamental goals of molecular electronics. In this dissertation, conductance measurements on DNA origami molecules were performed. A systematic study on the charge transport properties through the directly coupled DNA guanine-quadruplexes (G-quadruplexes) to gold electrodes was conducted by changing the number of the G-quads. The single-molecule break junction (SMBJ) technique is a valuable tool that could detect a small population of G-quad molecules that are not possible to detect using conventional techniques such as Gel electrophoresis or Circular dichroism. The SMBJ technique has been used to measure the conductance values for double-stranded DNA (dsDNA) and DNA: RNA hybrids by bridging the molecule between metal electrodes in an aqueous solution.

First, six strands of DNA hybridized in an aqueous solution with magnesium ions form a four-helix bundle of DNA origami. The nanotube structure is 10 nm long, and 70% of the molecule is rich in guanine. The conductance value of the DNA origami is relatively high compared to 10 nm double-stranded DNA. The development of flyfishing mode along with the blink and pull technique suggests that the charge is transported through the π-stack of the origami. Also, the thiols on the DNA origami provide mechanical stability to the molecule and have less impact on the conductance value.

Next, a series of DNA G-quadruplex with various numbers of G-quartets was studied. The conductance value of the G-quadruplexes is weakly length-dependent, and the fitting of the experimental results suggests that the transport mechanism is partially-coherence corrected hopping. The density functional theory (DFT) calculations show that the highest occupied molecular orbital (HOMO) is delocalized across the G-quartets.

Finally, extending the use of SMBJ beyond fundamental charge transport studies, detecting G-quadruplex structures in a mixture with double-stranded DNA (dsDNA) was performed. Other techniques such as gel electrophoresis or circular dichroism (CD) may not detect a low concentration of G-quadruplex structures in a mixture with dsDNA. The detection of G-quadruplex presence in a solution is significant for gene expression and genetic diseases. The molecular-based approach using the SMBJ technique shows that the conductance value of the G-quadruplex can be measured in a mixture with dsDNA structures.

5.2. Outlook

This work may represent one step in the journey towards future DNA-based devices. For instance, DNA-storage devices are less expensive and more energy-efficient compared to nowadays storage technologies. Also, DNA units in the size of a poppy seed or even smaller could hold zettabytes of information. DNA origami could be used as a molecular wire to interconnect multiple DNA units. Moreover, the weak length-dependent G-quadruplex may serve as a contact between functional DNA units and the DNA origami.

The biological significance of G-quadruplex, including gene regulation and drug targets for many genetic diseases, urges the development of a single-molecule sensing platform. Micro-electromechanical- system break junction (MEMS-BJ) could be applied in conjunction with G-

quadruplex to develop an on-chip, label-free, and low-concentration sensing platform. However, challenges exist on multiple fronts, such as a thorough understanding of the charge transport in many different G-quadruplex topologies and environments.

References:

(1)   Aviram, A.; Ratner, M. A. Molecular Rectifiers. *Chem. Phys. Lett.* **1974**, *29* (2), 277–283. https://doi.org/10.1016/0009-2614(74)85031-1.

(2)   Binnig, G.; Rohrer, H. Scanning Tunneling Microscopy. *Surf. Sci.* **1983**, *126* (1–3), 236–244. https://doi.org/10.1016/0039-6028(83)90716-1.

(3)   Ramachandran, G. K.; Hopson, T. J.; Rawtett, A. M.; Nagahara, L. A.; Primak, A.; Lindsay, S. M. A Bond-Fluctuation Mechanism for Stochastic Switching in Wired Molecules. *Science (80-.).* **2003**, *300* (5624), 1413–1416. https://doi.org/10.1126/SCIENCE.1083825.

(4)   Xu, B.; Tao, N. J. Measurement of Single-Molecule Resistance by Repeated Formation of Molecular Junctions. *Science* **2003**, *301* (5637), 1221–1223. https://doi.org/10.1126/science.1087481.

(5)   Reed, M. A.; Zhou, C.; Muller, C. J.; Burgin, T. P.; Tour, J. M. Conductance of a Molecular Junction. *Science (80-.).* **1997**, *278* (5336), 252–254. https://doi.org/10.1126/science.278.5336.252.

(6)   Smit, R. H. M.; Noat, Y.; Untiedt, C.; Lang, N. D.; van Hemert, M. C.; van Ruitenbeek, J. M. Measurement of the Conductance of a Hydrogen Molecule. *Nat. 2002 4196910* **2002**, *419* (6910), 906–909. https://doi.org/10.1038/nature01103.

(7)   J. G. Kushmerick, *; J. Naciri; J. C. Yang, and; Shashidhar, R. Conductance Scaling of Molecular Wires in Parallel. *Nano Lett.* **2003**, *3* (7), 897–900. https://doi.org/10.1021/NL034201N.

(8)   Chen, J.; Reed, M. A.; Rawlett, A. M.; Tour, J. M. Large On-off Ratios and Negative Differential Resistance in a Molecular Electronic Device. *Science (80-.).* **1999**, *286* (5444), 1550–1552. https://doi.org/10.1126/SCIENCE.286.5444.1550.

(9)   Bonifas, A. P.; McCreery, R. L. 'Soft' Au, Pt and Cu Contacts for Molecular Junctions through Surface-Diffusion-Mediated Deposition. *Nat. Nanotechnol. 2010 58* **2010**, *5* (8), 612–617. https://doi.org/10.1038/nnano.2010.115.

(10)   Park, J.; Pasupathy, A. N.; Goldsmith, J. I.; Chang, C.; Yaish, Y.; Petta, J. R.; Rinkoski, M.; Sethna, J. P.; Abruña, H. D.; McEuen, P. L.; et al. Coulomb Blockade and the Kondo Effect in Single-Atom Transistors. *Nat. 2002 4176890* **2002**, *417* (6890), 722–725. https://doi.org/10.1038/nature00791.

(11)   Cao, Y.; Dong, S.; Liu, S.; He, L.; Gan, L.; Yu, X.; Steigerwald, M. L.; Wu, X.; Liu, Z.; Guo, X. Building High-Throughput Molecular Junctions Using Indented Graphene Point Contacts. *Angew. Chemie* **2012**, *124* (49), 12394–12398. https://doi.org/10.1002/ANGE.201205607.

(12)   Guo, X.; Small, J. P.; Klare, J. E.; Wang, Y.; Purewal, M. S.; Tam, I. W.; Hong, B. H.; Caldwell, R.; Huang, L.; O'Brien, S.; et al. Covalently Bridging-Gaps in Single-Walled Carbon Nanotubes with Conducting Molecules. *Science (80-.).* **2006**, *311* (5759), 356–359. https://doi.org/10.1126/SCIENCE.1120986.

(13)   Xiang, J.; Liu, B.; Wu, S.-T.; Ren, B.; Yang, F.-Z.; Mao, B.-W.; Chow, Y. L.; Tian, Z.-Q. A Controllable Electrochemical Fabrication of Metallic Electrodes with a Nanometer/Angstrom-Sized Gap Using an Electric Double Layer as Feedback. *Angew. Chemie* **2005**, *117* (8), 1291–1294. https://doi.org/10.1002/ANGE.200461797.

(14)   Hines, T.; Diez-Perez, I.; Hihath, J.; Liu, H.; Wang, Z.-S.; Zhao, J.; Zhou, G.; Müllen, K.; Tao, N. Transition from Tunneling to Hopping in Single Molecular Junctions by Measuring Length and Temperature Dependence. *J. Am. Chem. Soc.* **2010**, *132* (33), 11658–11664. https://doi.org/10.1021/ja1040946.

(15)   Dell, E. J.; Capozzi, B.; Xia, J.; Venkataraman, L.; Campos, L. M. Molecular Length Dictates the Nature of Charge Carriers in Single-Molecule Junctions of Oxidized Oligothiophenes. *Nat Chem* **2015**, *7* (3), 209–214. https://doi.org/10.1038/nchem.2160.

(16)   Li, Y.; Xiang, L.; Palma, J. L.; Asai, Y.; Tao, N. Thermoelectric Effect and Its Dependence on Molecular Length and Sequence in Single DNA Molecules. *Nat. Commun.* **2016**, *7*, 1–8. https://doi.org/10.1038/ncomms11294.

(17)   Kiguchi, M.; Ohto, T.; Fujii, S.; Sugiyasu, K.; Nakajima, S.; Takeuchi, M.; Nakamura, H. Single Molecular Resistive Switch Obtained via Sliding Multiple Anchoring Points and Varying Effective Wire Length. *J Am Chem Soc* **2014**, *136* (20), 7327–7332. https://doi.org/10.1021/ja413104g.

(18)   Agraït, N.; Hodgson, A.; Anderson, H. L.; Sadeghi, H.; Noori, M.; Limburg, B.; Alanazy, A.; Leary, E.; Esdaile, L. J.; Grace, I.; et al. Bias-Driven Conductance Increase with Length in Porphyrin Tapes. *J. Am. Chem. Soc.* **2018**, *140* (40), 12877–12883. https://doi.org/10.1021/jacs.8b06338.

(19)   Swasey, S. M.; Gwinn, E. G. Silver-Mediated Base Pairings: Towards Dynamic DNA Nanostructures with Enhanced Chemical and Thermal Stability. *New J. Phys.* **2016**, *18* (4). https://doi.org/10.1088/1367-2630/18/4/045008.

(20)   Cai, Z.; Lo, W. Y.; Zheng, T.; Li, L.; Zhang, N.; Hu, Y.; Yu, L. Exceptional Single-Molecule Transport Properties of Ladder-Type Heteroacene Molecular Wires. *J. Am. Chem. Soc.* **2016**, *138* (33), 10630–10635. https://doi.org/10.1021/jacs.6b05983.

(21)   Beall, E.; Ulku, S.; Liu, C.; Wierzbinski, E.; Zhang, Y.; Bae, Y.; Zhang, P.; Achim, C.; Beratan, D. N.; Waldeck, D. H. Effects of the Backbone and Chemical Linker on the Molecular Conductance of Nucleic Acid Duplexes. *J. Am. Chem. Soc.* **2017**, *139* (19), 6726–6735. https://doi.org/10.1021/jacs.7b02260.

(22)   Walkey, M. C.; Peiris, C. R.; Ciampi, S.; C. Aragonès, A.; Domínguez-Espíndola, R. B.; Jago, D.; Pulbrook, T.; Skelton, B. W.; Sobolev, A. N.; Díez Pérez, I.; et al. Chemically and Mechanically Controlled Single-Molecule Switches Using Spiropyrans. *ACS Appl. Mater. Interfaces* **2019**, *11* (40), 36886–36894. https://doi.org/10.1021/acsami.9b11044.

(23)   Kay, N. J.; Higgins, S. J.; Jeppesen, J. O.; Leary, E.; Lycoops, J.; Ulstrup, J.; Nichols, R. J. Single-Molecule Electrochemical Gating in Ionic Liquids. *J Am Chem Soc* **2012**, *134* (40), 16817–16826. https://doi.org/10.1021/ja307407e.

(24)   Nichols, R. J.; Higgins, S. J. Single Molecule Nanoelectrochemistry in Electrical Junctions. *Acc. Chem. Res.* **2016**, *49* (11), 2640–2648. https://doi.org/10.1021/acs.accounts.6b00373.

(25)   Xuan, S.; Meng, Z.; Wu, X.; Wong, J.-R.; Devi, G.; Yeow, E. K. L.; Shao, F. Efficient DNA-Mediated Electron Transport in Ionic Liquids. *ACS Sustain. Chem. Eng.* **2016**, *4* (12), 6703–6711. https://doi.org/10.1021/acssuschemeng.6b01605.

(26)   Diez-Perez, I.; Li, Z. H.; Guo, S. Y.; Madden, C.; Huang, H. L.; Che, Y. K.; Yang, X. M.; Zang, L.; Tao, N. J. Ambipolar Transport in an Electrochemically Gated Single-Molecule Field-Effect Transistor. *ACS Nano* **2012**, *6* (8), 7044–7052. https://doi.org/10.1021/nn302090t.

(27)   Pobelov, I. V; Li, Z. H.; Wandlowski, T. Electrolyte Gating in Redox-Active Tunneling

Junctions-An Electrochemical STM Approach. *J Am Chem Soc* **2008**, *130* (47), 16045–16054. https://doi.org/10.1021/ja8054194.

(28)   Baghernejad, M.; Zhao, X.; Baruël Ørnsø, K.; Füeg, M.; Moreno-García, P.; Rudnev, A. V.; Kaliginedi, V.; Vesztergom, S.; Huang, C.; Hong, W.; et al. Electrochemical Control of Single-Molecule Conductance by Fermi-Level Tuning and Conjugation Switching. *J. Am. Chem. Soc.* **2014**, *136* (52), 17922–17925. https://doi.org/10.1021/ja510335z.

(29)   Fuechsle, M.; Miwa, J. A.; Mahapatra, S.; Ryu, H.; Lee, S.; Warschkow, O.; Hollenberg, L. C. L.; Klimeck, G.; Simmons, M. Y. A Single-Atom Transistor. *Nat. Nanotechnol. 2012 74* **2012**, *7* (4), 242–246. https://doi.org/10.1038/nnano.2012.21.

(30)   Alexandre R. Champagne; Abhay N. Pasupathy, † and; Ralph*, D. C. Mechanically Adjustable and Electrically Gated Single-Molecule Transistors. *Nano Lett.* **2005**, *5* (2), 305–308. https://doi.org/10.1021/NL0480619.

(31)   Donarini, A.; Begemann, G.; Grifoni, M. All-Electric Spin Control in Interference Single Electron Transistors. *Nano Lett.* **2009**, *9* (8), 2897–2902. https://doi.org/10.1021/NL901199P.

(32)   Guo, C.; Wang, K.; Zerah-Harush, E.; Hamill, J.; Wang, B.; Dubi, Y.; Xu, B. Molecular Rectifier Composed of DNA with High Rectification Ratio Enabled by Intercalation. *Nat. Chem.* **2016**, *8* (5), 484–490. https://doi.org/10.1038/nchem.2480.

(33)   Kornilovitch, P. E.; Bratkovsky, A. M.; Stanley Williams, R. Current Rectification by Molecules with Asymmetric Tunneling Barriers. *Phys. Rev. B* **2002**, *66* (16). https://doi.org/10.1103/PhysRevB.66.165436.

(34)   Díez-Pérez, I.; Hihath, J.; Lee, Y.; Yu, L.; Adamska, L.; Kozhushner, M. A.; Oleynik, I. I.; Tao, N. Rectification and Stability of a Single Molecular Diode with Controlled Orientation. *Nat. Chem. 2009 18* **2009**, *1* (8), 635–641. https://doi.org/10.1038/nchem.392.

(35)   Pascual, J. I.; Méndez, J.; Gómez-Herrero, J.; Baró, A. M.; García, N.; Binh, V. T. Quantum Contact in Gold Nanostructures by Scanning Tunneling Microscopy. *Phys. Rev. Lett.* **1993**, *71* (12), 1852. https://doi.org/10.1103/PhysRevLett.71.1852.

(36)   Agraït, N.; Rodrigo, J. G.; Vieira, S. Conductance Steps and Quantization in Atomic-Size Contacts. *Phys. Rev. B* **1993**, *47* (18), 12345. https://doi.org/10.1103/PhysRevB.47.12345.

(37)   Landauer, R. Spatial Variation of Currents and Fields Due to Localized Scatterers in Metallic Conduction. *IBM J. Res. Dev.* **2010**, *1* (3), 223–231. https://doi.org/10.1147/rd.13.0223.

(38)   Li, Y.; Artes, J. M.; Hihath, J. Long-Range Charge Transport in Adenine-Stacked RNA:DNA Hybrids. *Small* **2016**, *12* (4), 432–437. https://doi.org/10.1002/smll.201502399.

(39)   Xiang, L.; Palma, J. L.; Bruot, C.; Mujica, V.; Ratner, M. A.; Tao, N. Intermediate Tunnelling-Hopping Regime in DNA Charge Transport. *Nat Chem* **2015**, *7* (3), 221–226. https://doi.org/10.1038/nchem.2183.

(40)   Buttiker, M. COHERENT AND SEQUENTIAL TUNNELING IN SERIES BARRIERS. *IBM J. Res. Dev.* **1988**, *32* (1), 63–75. https://doi.org/10.1147/rd.321.0063.

(41)   Kahr, B. Polarization in France. *Chirality* **2018**, *30* (4), 351–368. https://doi.org/10.1002/CHIR.22818.

(42)   Kahr, B. Better than CD: Eugénie Cotton (1881-1967). *Chirality* **2020**, *32* (5), 652–660. https://doi.org/10.1002/CHIR.23215.

(43)   Woody, R. W. [4] Circular Dichroism. *Methods Enzymol.* **1995**, *246* (C), 34–71.

https://doi.org/10.1016/0076-6879(95)46006-3.

(44) Valev - Ellipticity https://people.bath.ac.uk/vkv23/English/RechercheT3a.htm (accessed Sep 13, 2021).

(45) Circular Dichroism - Chemistry LibreTexts https://chem.libretexts.org/Bookshelves/Physical_and_Theoretical_Chemistry_Textbook_Maps/Supplemental_Modules_(Physical_and_Theoretical_Chemistry)/Spectroscopy/Electronic_Spectroscopy/Circular_Dichroism (accessed Sep 13, 2021).

(46) Discovery of the structure of DNA (article) | Khan Academy https://www.khanacademy.org/science/biology/dna-as-the-genetic-material/dna-discovery-and-structure/a/discovery-of-the-structure-of-dna (accessed Sep 13, 2021).

(47) Sinden, R. R. *DNA Structure and Function*; Academic Press; 1st edition.

(48) Kypr, J.; Kejnovská, I.; Bednářová, K.; Vorlíčková, M. Circular Dichroism Spectroscopy of Nucleic Acids. *Compr. Chiroptical Spectrosc.* **2012**, No. February, 575–586. https://doi.org/10.1002/9781118120392.ch17.

(49) Štefl, R.; Trantírek, L.; Vorlíčková, M.; Koča, J.; Sklenář, V.; Kypr, J. A-like Guanine-Guanine Stacking in the Aqueous DNA Duplex of d(GGGGCCCC). *J. Mol. Biol.* **2001**, *307* (2), 513–524. https://doi.org/10.1006/jmbi.2001.4484.

(50) Kypr, J.; Kejnovská, I.; Renčiuk, D.; Vorlíčková, M. Circular Dichroism and Conformational Polymorphism of DNA. *Nucleic Acids Res.* **2009**, *37* (6), 1713–1725. https://doi.org/10.1093/nar/gkp026.

(51) Alexeev, D. G.; Lipanov, A. A.; Ya. Skuratovskii, I. Poly(DA)Ṁpoly(DT) Is a B-Type Double Helix with a Distinctively Narrow Minor Groove. *Nat. 1987 3256107* **1987**, *325* (6107), 821–823. https://doi.org/10.1038/325821a0.

(52) Nelson, H. C. M.; Finch, J. T.; Luisi, B. F.; Klug, A. The Structure of an Oligo(DA)·oligo(DT) Tract and Its Biological Implications. *Nat. 1987 3306145* **1987**, *330* (6145), 221–226. https://doi.org/10.1038/330221a0.

(53) Artés, J. M.; Li, Y.; Qi, J.; Anantram, M. P.; Hihath, J. Conformational Gating of DNA Conductance. *Nat. Commun.* **2015**, *6*. https://doi.org/10.1038/ncomms9870.

(54) Pohl, F. M.; Jovin, T. M. Salt-Induced Co-Operative Conformational Change of a Synthetic DNA: Equilibrium and Kinetic Studies with Poly(DG-DC). *J. Mol. Biol.* **1972**, *67* (3), 375–396. https://doi.org/10.1016/0022-2836(72)90457-3.

(55) Wang, A. H.-J.; Quigley, G. J.; Kolpak, F. J.; Crawford, J. L.; van Boom, J. H.; van der Marel, G.; Rich, A. Molecular Structure of a Left-Handed Double Helical DNA Fragment at Atomic Resolution. *Nat. 1979 2825740* **1979**, *282* (5740), 680–686. https://doi.org/10.1038/282680a0.

(56) Drew, H.; Takano, T.; Tanaka, S.; Itakura, K.; Dickerson, R. E. High-Salt d(CpGpCpG), a Left-Handed Z′ DNA Double Helix. *Nat. 1980 2865773* **1980**, *286* (5773), 567–573. https://doi.org/10.1038/286567a0.

(57) Bošković, F.; Zhu, J.; Chen, K.; Keyser, U. F. Monitoring G-Quadruplex Formation with DNA Carriers and Solid-State Nanopores. *Nano Lett.* **2019**, *19* (11), 7996–8001. https://doi.org/10.1021/acs.nanolett.9b03184.

(58) Nishio, M.; Tsukakoshi, K.; Ikebukuro, K. G-Quadruplex: Flexible Conformational Changes by Cations, PH, Crowding and Its Applications to Biosensing. *Biosensors and Bioelectronics*. Elsevier Ltd April 15, 2021, p 113030. https://doi.org/10.1016/j.bios.2021.113030.

(59) Paramasivan, S.; Rujan, I.; Bolton, P. H. Circular Dichroism of Quadruplex DNAs:

Applications to Structure, Cation Effects and Ligand Binding. *Methods* **2007**, *43* (4), 324–331. https://doi.org/10.1016/J.YMETH.2007.02.009.

(60) Huppert, J. L. Four-Stranded Nucleic Acids: Structure, Function and Targeting of G-Quadruplexes. *Chem. Soc. Rev.* **2008**, *37* (7), 1375–1384. https://doi.org/10.1039/b702491f.

(61) Vorlíčková, M.; Kejnovská, I.; Sagi, J.; Renčiuk, D.; Bednářová, K.; Motlová, J.; Kypr, J. Circular Dichroism and Guanine Quadruplexes. *Methods* **2012**, *57* (1), 64–75. https://doi.org/10.1016/j.ymeth.2012.03.011.

(62) Parkinson, G. N.; Lee, M. P. H.; Neidle, S. Crystal Structure of Parallel Quadruplexes from Human Telomeric DNA. *Nature* **2002**, *417* (6891), 876–880. https://doi.org/10.1038/nature755.

(63) del Villar-Guerra, R.; Trent, J. O.; Chaires, J. B. G-Quadruplex Secondary Structure Obtained from Circular Dichroism Spectroscopy. *Angew. Chemie Int. Ed.* **2018**, *57* (24), 7171–7175. https://doi.org/10.1002/anie.201709184.

(64) Gray, D. M.; Wen, J.-D.; Gray, C. W.; Repges, R.; Repges, C.; Raabe, G.; Fleischhauer, J. Measured and Calculated CD Spectra of G-Quartets Stacked with the Same or Opposite Polarities. *Chirality* **2008**, *20* (3–4), 431–440. https://doi.org/10.1002/chir.20455.

(65) Vorlíčková, M.; Kejnovská, I.; Bednářová, K.; Renčiuk, D.; Kypr, J. Circular Dichroism Spectroscopy of DNA: From Duplexes to Quadruplexes. *Chirality* **2012**, *24* (9), 691–698. https://doi.org/10.1002/chir.22064.

(66) Pascale Hazel, †; Julian Huppert, ‡; Shankar Balasubramanian, ‡ and; Stephen Neidle*, †. Loop-Length-Dependent Folding of G-Quadruplexes. *J. Am. Chem. Soc.* **2004**, *126* (50), 16405–16415. https://doi.org/10.1021/JA045154J.

(67) Burge, S.; Parkinson, G. N.; Hazel, P.; Todd, A. K.; Neidle, S. Quadruplex DNA: Sequence, Topology and Structure. *Nucleic Acids Res.* **2006**, *34* (19), 5402–5415. https://doi.org/10.1093/nar/gkl655.

(68) Stefano Masiero; Roberta Trotta; Silvia Pieraccini; Tito, S. D.; Rosaria Perone; Antonio Randazzo; Piero Spada, G. A Non-Empirical Chromophoric Interpretation of CD Spectra of DNA G-Quadruplex Structures. *Org. Biomol. Chem.* **2010**, *8* (12), 2683–2692. https://doi.org/10.1039/C003428B.

(69) Liu, S.-P.; Weisbrod, S. H.; Tang, Z.; Marx, A.; Scheer, E.; Erbe, A. Direct Measurement of Electrical Transport Through G-Quadruplex DNA with Mechanically Controllable Break Junction Electrodes. *Angew. Chemie Int. Ed.* **2010**, *49* (19), 3313–3316. https://doi.org/10.1002/anie.201000022.

(70) Xiang, D.; Jeong, H.; Lee, T.; Mayer, D. Mechanically Controllable Break Junctions for Molecular Electronics. *Adv. Mater.* **2013**, *25* (35), 4845–4867. https://doi.org/10.1002/ADMA.201301589.

(71) Moreland, J.; Ekin, J. W. Electron Tunneling Experiments Using Nb-Sn '"Break"' Junctions. *J. Appl. Phys.* **1998**, *58* (10), 3888. https://doi.org/10.1063/1.335608.

(72) Livshits, G. I.; Stern, A.; Rotem, D.; Borovok, N.; Eidelshtein, G.; Migliore, A.; Penzo, E.; Wind, S. J.; Di Felice, R.; Skourtis, S. S.; et al. Long-Range Charge Transport in Single G-Quadruplex DNA Molecules. *Nat Nanotechnol* **2014**, *9* (12), 1040–1046. https://doi.org/10.1038/nnano.2014.246.

(73) Seeman, N. C. Nucleic Acid Junctions and Lattices. *J. Theor. Biol.* **1982**, *99* (2), 237–247. https://doi.org/10.1016/0022-5193(82)90002-9.

(74) P. Goodman, R.; M. Berry, R.; J. Turberfield, A. The Single-Step Synthesis of a DNA

Tetrahedron. *Chem. Commun.* **2004**, *0* (12), 1372–1373.
https://doi.org/10.1039/B402293A.

(75)   Shih, W. M.; Quispe, J. D.; Joyce, G. F. A 1.7-Kilobase Single-Stranded DNA That Folds
into a Nanoscale Octahedron. *Nat. 2004 4276975* **2004**, *427* (6975), 618–621.
https://doi.org/10.1038/nature02307.

(76)   Aldaye, F. A.; Palmer, A. L.; Sleiman, H. F. Assembling Materials with DNA as the
Guide. *Science (80-.).* **2008**, *321* (5897), 1795–1799.
https://doi.org/10.1126/SCIENCE.1154533.

(77)   Rothemund, P. W. K. Folding DNA to Create Nanoscale Shapes and Patterns. *Nature*
2006, *440* (7082), 297–302. https://doi.org/10.1038/nature04586.

(78)   Douglas, S. M.; Dietz, H.; Liedl, T.; Högberg, B.; Graf, F.; Shih, W. M. Self-Assembly of
DNA into Nanoscale Three-Dimensional Shapes. *Nature* **2009**, *459* (7245), 414–418.
https://doi.org/10.1038/nature08016.

(79)   Douglas, S. M.; Marblestone, A. H.; Teerapittayanon, S.; Vazquez, A.; Church, G. M.;
Shih, W. M. Rapid Prototyping of 3D DNA-Origami Shapes with CaDNAno. *Nucleic
Acids Res.* **2009**, *37* (15), 5001–5006. https://doi.org/10.1093/NAR/GKP436.

(80)   Zhang, Q.; Jiang, Q.; Li, N.; Dai, L.; Liu, Q.; Song, L.; Wang, J.; Li, Y.; Tian, J.; Ding,
B.; et al. DNA Origami as an In Vivo Drug Delivery Vehicle for Cancer Therapy. *ACS
Nano* **2014**, *8* (7), 6633–6643. https://doi.org/10.1021/NN502058J.

(81)   Gu, H.; Chao, J.; Xiao, S.-J.; Seeman, N. C. A Proximity-Based Programmable DNA
Nanoscale Assembly Line. *Nat. 2010 4657295* **2010**, *465* (7295), 202–205.
https://doi.org/10.1038/nature09026.

(82)   Roller, E.-M.; Besteiro, L. V.; Pupp, C.; Khorashad, L. K.; Govorov, A. O.; Liedl, T.
Hotspot-Mediated Non-Dissipative and Ultrafast Plasmon Passage. *Nat. Phys. 2017 138*
2017, *13* (8), 761–765. https://doi.org/10.1038/nphys4120.

(83)   Ghomian, T.; Jeong, H.; Pan, V.; Celik, K.; Alangari, M.; Ke, Y.; Hihath, J. High-
Throughput Dielectrophoretic Trapping and Detection of DNA Origami. *Adv. Mater.
Interfaces* **2021**, *8* (5), 2001476. https://doi.org/10.1002/ADMI.202001476.

(84)   Naskar, S.; Gosika, M.; Joshi, H.; Maiti, P. K. Tuning the Stability of DNA Nanotubes
with Salt. *J. Phys. Chem. C* **2019**, *123* (14), 9461–9470.
https://doi.org/10.1021/acs.jpcc.8b10156.

(85)   Liu, D.; Park, S. H.; Reif, J. H.; Labean, T. H. *DNA Nanotubes Self-Assembled from
Triple-Crossover Tiles as Templates for Conductive Nanowires*; 2004.

(86)   Teschome, B.; Facsko, S.; Schönherr, T.; Kerbusch, J.; Keller, A.; Erbe, A. Temperature-
Dependent Charge Transport through Individually Contacted DNA Origami-Based Au
Nanowires. *Langmuir* **2016**, *32* (40), 10159–10165.
https://doi.org/10.1021/ACS.LANGMUIR.6B01961.

(87)   Yan, H.; Park, S. H.; Finkelstein, G.; Reif, J. H.; LaBean, T. H. DNA-Templated Self-
Assembly of Protein Arrays and Highly Conductive Nanowires. *Science (80-.).* **2003**, *301*
(5641), 1882–1884. https://doi.org/10.1126/science.1089389.

(88)   Karsisiotis, A. I.; O'kane, C.; Webba Da Silva, M. DNA Quadruplex Folding Formalism-
A Tutorial on Quadruplex Topologies. **2013**. https://doi.org/10.1016/j.ymeth.2013.06.004.

(89)   D, R.; HJ, L. G-Quadruplexes and Their Regulatory Roles in Biology. *Nucleic Acids Res.*
2015, *43* (18), 8627–8637. https://doi.org/10.1093/NAR/GKV862.

(90)   Zhang, Y.; Zhang, W. B.; Liu, C.; Zhang, P.; Balaeff, A.; Beratan, D. N. DNA Charge
Transport: Moving beyond 1D. *Surf. Sci.* **2016**, *652*, 33–38.

https://doi.org/10.1016/j.susc.2016.03.011.

(91) Guo, A.-M.; Yang, Z.; Zhu, H.-J.; Xiong, S.-J. Influence of Backbone on the Charge Transport Properties of G4-DNA Molecules: A-Based Calculation. *J. Phys. Condens. Matter* **2010**, *22* (6), 065102. https://doi.org/10.1088/0953-8984/22/6/065102.

(92) Kubař, T.; Woiczikowski, P. B.; Cuniberti, G.; Elstner, M. Efficient Calculation of Charge-Transfer Matrix Elements for Hole Transfer in DNA. *J. Phys. Chem. B* **2008**, *112* (26), 7937–7947. https://doi.org/10.1021/JP801486D.

(93) Wu, J.; Meng, Z.; Lu, Y.; Shao, F. Efficient Long-Range Hole Transport Through G-Quadruplexes. *Chem. - A Eur. J.* **2017**, *23* (56), 13980–13985. https://doi.org/10.1002/chem.201702478.

(94) Thazhathveetil, A. K.; Harris, M. A.; Young, R. M.; Wasielewski, M. R.; Lewis, F. D. Efficient Charge Transport via DNA G-Quadruplexes. *J. Am. Chem. Soc.* **2017**, *139* (5), 1730–1733. https://doi.org/10.1021/jacs.6b10265.

(95) Balagurumoorthy, P.; Brahmachari, S. K.; Mohanty, D.; Bansal, M.; Sasisekharan, V. Hairpin and Parallel Quartet Structures for Telomeric Sequences. *Nucleic Acids Res.* **1992**, *20* (15), 4061–4067. https://doi.org/10.1093/NAR/20.15.4061.

(96) Thazhathveetil, A. K.; Harris, M. A.; Young, R. M.; Wasielewski, M. R.; Lewis, F. D. Efficient Charge Transport via DNA G-Quadruplexes. *J. Am. Chem. Soc* **2017**, *139*, 1730–1733. https://doi.org/10.1021/jacs.6b10265.

(97) Jia, C.; Migliore, A.; Xin, N.; Huang, S.; Wang, J.; Yang, Q.; Wang, S.; Chen, H.; Wang, D.; Feng, B.; et al. Covalently Bonded Single-Molecule Junctions with Stable and Reversible Photoswitched Conductivity. *Science (80-.).* **2016**, *352* (6292), 1443–1445. https://doi.org/10.1126/SCIENCE.AAF6298.

(98) Drummond, T. G.; Hill, M. G.; Barton, J. K. Electrochemical DNA Sensors. *Nature Biotechnology*. 2003. https://doi.org/10.1038/nbt873.

(99) Kamyshny, A.; Magdassi, S. Conductive Nanomaterials for Printed Electronics. *Small* **2014**, *10* (17), 3515–3535. https://doi.org/10.1002/SMLL.201303000.

(100) Okawa, Y.; Mandal, S. K.; Hu, C.; Tateyama, Y.; Goedecker, S.; Tsukamoto, S.; Hasegawa, T.; Gimzewski, J. K.; Aono, M. Chemical Wiring and Soldering toward All-Molecule Electronic Circuitry. *J Am Chem Soc* **2011**, *133* (21), 8227–8233. https://doi.org/10.1021/ja111673x.

(101) Vilan, A.; Aswal, D.; Cahen, D. Large-Area, Ensemble Molecular Electronics: Motivation and Challenges. *Chem. Rev.* **2017**, *117* (5), 4248–4286. https://doi.org/10.1021/acs.chemrev.6b00595.

(102) Woiczikowski, P. B.; Kubař, T.; Gutiérrez, R.; Cuniberti, G.; Elstner, M. Structural Stability versus Conformational Sampling in Biomolecular Systems: Why Is the Charge Transfer Efficiency in G4-DNA Better than in Double-Stranded DNA? *J. Chem. Phys.* **2010**, *133* (3), 035103. https://doi.org/10.1063/1.3460132.

(103) Paramasivan, S.; Rujan, I.; Bolton, P. H. Circular Dichroism of Quadruplex DNAs: Applications to Structure, Cation Effects and Ligand Binding. *Methods* **2007**, *43* (4), 324–331. https://doi.org/10.1016/j.ymeth.2007.02.009.

(104) Guédin, A.; Gros, J.; Alberti, P.; Mergny, J. L. How Long Is Too Long? Effects of Loop Size on G-Quadruplex Stability. *Nucleic Acids Res.* **2010**, *38* (21), 7858–7868. https://doi.org/10.1093/nar/gkq639.

(105) Li, Y.; Artes, J. M.; Qi, J.; Morelan, I. A.; Feldstein, P.; Anantram, M. P.; Hihath, J. Comparing Charge Transport in Oligonucleotides: RNA:DNA Hybrids and DNA

Duplexes. *J Phys Chem Lett* **2016**, *7* (10), 1888–1894.
https://doi.org/10.1021/acs.jpclett.6b00749.

(106)   Wang, K.; Hamill, J. M.; Wang, B.; Guo, C.; Jiang, S.; Huang, Z.; Xu, B. Structure
Determined Charge Transport in Single DNA Molecule Break Junctions. *Chem. Sci.* **2014**,
5 (9), 3425–3431. https://doi.org/10.1039/c4sc00888j.

(107)   Dulić, D.; Tuukkanen, S.; Chung, C.-L.; Isambert, A.; Lavie, P.; Filoramo, A. Direct
Conductance Measurements of Short Single DNA Molecules in Dry Conditions.
Nanotechnology **2009**, *20* (11), 115502. https://doi.org/10.1088/0957-4484/20/11/115502.

(108)   Li, Y.; Artés, J. M.; Demir, B.; Gokce, S.; Mohammad, H. M.; Alangari, M.; Anantram,
M. P.; Oren, E. E.; Hihath, J. Detection and Identification of Genetic Material via Single-
Molecule Conductance. *Nat. Nanotechnol.* **2018**, 1. https://doi.org/10.1038/s41565-018-
0285-x.

(109)   Bingqian Xu, †; Peiming Zhang, ‡; Xiulan Li, † and; Nongjian Tao*, †. Direct
Conductance Measurement of Single DNA Molecules in Aqueous Solution. **2004**.
https://doi.org/10.1021/NL0494295.

(110)   Kwok, C. K.; Merrick, C. J. G-Quadruplexes: Prediction, Characterization, and Biological
Application. *Trends Biotechnol.* **2017**, *35* (10), 997–1013.
https://doi.org/10.1016/J.TIBTECH.2017.06.012.

(111)   Fujii, T.; Podbevšek, P.; Plavec, J.; Sugimoto, N. Effects of Metal Ions and Cosolutes on
G-Quadruplex Topology. *J. Inorg. Biochem.* **2017**, *166*, 190–198.
https://doi.org/10.1016/j.jinorgbio.2016.09.001.